Macromolecules

pubs.acs.org/Macromolecules Article

Linear Viscoelasticity of Model Vitrimers: Decoding the Interplay between Bond Exchange and Segmental Dynamics

Hao Wang, Nuofei Jiang, Rongchun Zhang, Renaud Nicolaÿ, Charles-André Fustin, and Evelyne Van Ruymbeke*

Cite This: Macromolecules 2026, 59, 2818−2834 Read Online

ACCESS | Metrics & More | Article Recommendations | Supporting Information

ABSTRACT: The viscoelastic behavior of vitrimers is closely linked to the nature of the dynamic bonds, the functional group density and distribution, and the topology of the network. The aim of this study is to investigate the influence of segmental motion versus exchange dynamics on the viscoelastic response of vitrimers. To this end, we synthesized two unentangled model polyacrylate-based vitrimers with varying cross-linking densities, using a low-T_g poly(*n*-butyl acrylate) (P*n*BA) precursor and a bis-dioxaborolane cross-linker. Small-amplitude oscillatory shear (SAOS) experiments were conducted across a wide range of temperatures. In addition to the high frequency Rouse relaxation, the relaxation modulus of these vitrimers displays two relaxation processes, which show different dependencies on temperature. Consequently, thermo-rheological complexity is obtained in the viscoelastic data. To understand the origin of these two relaxation processes, we modified the time marching algorithm (TMA) tube-based model to account for the exchange dynamics of the reversible bonds, in order to separate the influence of the segmental dynamics from that of bond exchange dynamics. This analysis allows us to attribute the slower relaxation process to the relaxation of the molecular segments which are unable to move without activating the bond exchange mechanism, and the intermediate relaxation process to the relaxation of molecular segments containing dynamic bonds poorly trapped in the network. The temperature dependence of these relaxation processes was quantified and rationalized, combining the Arrhenius-like temperature dependence of the exchange dynamics and the WLF-like temperature dependence of the segmental dynamics. The influence of the molar mass of the precursor and of the cross-linker density is also discussed and considered in our model. This study brings new insights on how to understand and control the viscoelastic properties of vitrimers.

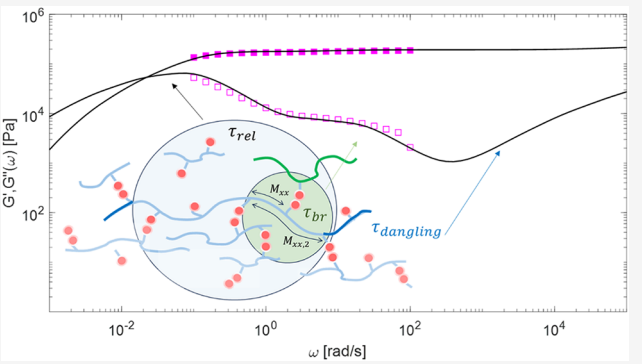

1. INTRODUCTION

Polymer networks based on reversible interactions, such as hydrogen bonding,[1,2] ionic interactions,[3,4] metal coordination,[5,6] and reversible chemical bonds,[7,8] typically exhibit a decrease of cross-linking density as temperature increases, which can lead to a solid to liquid transition. This decrease in connectivity leads to decreased mechanical properties and chemical resistance.[8−10] On the contrary, polymer networks composed of dynamic chemical junctions that undergo degenerate exchanges are characterized by a constant connectivity regardless of temperature.[11] Such polymer networks were coined vitrimers by Leibler and coworkers.[12] Vitrimers can combine the superior mechanical performances of thermosets with various advanced properties, such as shape-memory, interfacial adhesion or recyclability.[8,13,14]

In their seminal work, Leibler and coworkers demonstrated that the melt viscosity of vitrimers decreases gradually with temperature according to the Arrhenius law above the topology freezing temperature, T_v, which was defined as the temperature at which the melt viscosity of the vitrimer is equal to 10^{12} Pa·s.[11,12] Since then, vitrimers relying on different exchange chemistries and displaying various topologies have been described and studied.[8,14,15] Among them are polymer-based vitrimers, which we defined as vitrimers composed of polymer chains that do not contain dynamic bonds in their backbones. These vitrimers have proven to be of great interest for turning commodity thermoplastics into high performance materials[16−18] and for upcycling blends of polymers or plastic wastes.[19−21]

Understanding the viscoelasticity of vitrimers is crucial for enabling large-scale processing and expanding their potential applications. One of the major challenges is to comprehend the interplay of different temperature dependencies on the

Received: November 5, 2025
Revised: February 2, 2026
Accepted: February 9, 2026
Published: February 17, 2026

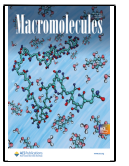

https://doi.org/10.1021/acs.macromol.5c03092
Macromolecules 2026, 59, 2818−2834

relaxation time of associative bonds and network strands. At temperatures near T_g, segmental and glassy dynamics dominate because the motion of the chains is restricted to the local level, and the exchange of dynamic bonds is hindered.[22] Within the temperature range between the T_g and T_v, the material behaves as an elastomer because the exchange reactions are slow enough to keep the network topology remains frozen.[14] At temperatures well above T_g and T_v, the exchange dynamics is expected to govern the relaxation of polymer chains in vitrimers. Due to this interplay between segmental dynamics and exchange dynamics, it is difficult to rationalize the viscoelastic properties of vitrimers. Many experimental or simulation studies have been carried out to enhance our understanding of their behavior.[23−28] In particular, Meng et al.[23] linked the dynamic bond exchange process to the total elastic energy density of vitrimers, and used this relationship to derive the rubber shear modulus and engineering tensile stress. Based on these findings, they proposed a method to determine the vitrimer relaxation time using small-strain oscillatory experiments and to determine the intrinsic exchange time through constant-load creep experiments, providing a systematic approach for analyzing vitrimer properties. Wu et al.[24] investigated a series of polymer-based vitrimers with low T_g and discussed their temperature dependent viscoelastic behaviors by looking at the possibility to build a master curve by superposing the viscoelastic data. Their findings suggest that the relaxation modulus of the vitrimer shows a weaker temperature (T) dependence compared to the segmental motions of polymer chains. This weak T dependence is believed to result from the lower activation energy of the bond exchange process, which governs the network relaxation in the presence of small molecules like the cross-linkers or the byproducts.[24] Khabaz and coworkers[25] utilized an MD/MC method to simulate the multitime scale viscoelasticity of vitrimers. They proposed to define the topology freezing transition temperature T_v as the transition temperature from a WLF-like behavior of the vitrimers at low temperatures, to an Arrhenius-like behavior, which describes the dynamics at high temperatures. Such transition temperature can be determined, based on the shift factors found by time−temperature superposition (tTS).

While the viscoelasticity of some vitrimers shows a very low T dependence, one could expect that for other vitrimers, similarly to supramolecular polymers, the dynamics of the exchangeable sites depends on the segmental motion of the chain backbone, as the functionalized groups cannot freely move since they are attached to the chain backbone. This could be one of the explanations for the complex thermo-rheological profile observed with some vitrimers. Ricarte and Shanbhag[28] investigated this question by looking at the influence of the distribution, density, and lifetime of stickers on the dynamics of unentangled vitrimers, and exploring the applicability of sticky Rouse based models. Their work suggests that the effective activation energy obtained from rheological measurements corresponds to the sum of the activation energies of the sticker exchange and of segmental dynamics in an unentangled associative vitrimer system. Additionally, the presence of free functional groups or dangling chain ends in vitrimers may further complicate their rheological behavior. Studies on epoxy- and PDMS-based vitrimers suggest a two-step relaxation mechanism, possibly associated with these free functional groups or active reaction sites.[29,30]

To gain a deeper understanding of the viscoelasticity of vitrimers, examining the relationship between their structure and their macroscopic characteristics by precisely tailoring the properties of the functional precursors represents a promising approach. The viscoelastic profile, including relaxation modes, plateau modulus, number of plateau zones, and terminal relaxation, is closely related to the nature of the dynamic bonds, the density of functional groups along the polymer backbone, and the length of the polymer precursor. This has been demonstrated through experimental data and theoretical models for reversible systems, such as ionic rubbers[3,31] or supramolecular networks.[6,32] As to vitrimers, few studies have investigated the impact of the distance between dynamic links, their distribution along the polymer backbone, or other structure-related variables on overall viscoelasticity. Soman and Evans explored a series of short-chain telechelic polyethylene cross-linked by boric acid to produce vitrimers and analyzed their thermo-rheological characteristics.[33] They found that the activation energy of these vitrimers is lower compared to that of vitrimers incorporating dioxaborolane side-functions, and increases monotonically with increasing cross-linking density.[33,34] Lessard et al. explored how the length of the precursor polymer chain influences the properties of vinylogous urethane[35] vitrimers.[36] At a constant density of dynamic bonds, the relaxation of vitrimers formed from precursors with a molar mass below M_e was found to be controlled by the exchange process and to follow a "Sticky Rouse" process.[37,38] Meanwhile, vitrimers obtained from precursors with molar masses well above M_e were found to follow a "Sticky Reptation" mechanism, similarly to supramolecular polymers.[39,40] Luo et al. employed tetra-PEG and presynthesized disulfide-containing polydimethylsiloxane to design a vitrimer with a precisely defined network, with a nearly uniform network mesh size.[41] They observed that the well-structured vitrimer exhibits superior mechanical performances compared to vitrimers and elastomers with randomly cross-linked networks, along with excellent reprocessability. By regulating the distribution of associative bonds along the polymer backbone, Sumerlin and coworkers also showed that the block copolymer vitrimers exhibit superior creep resistance.[42]

The present study aims to further understand the relationship between the composition of a vitrimer and its linear viscoelastic properties and thermo-rheological complexity. In particular, we investigate the interplay between polymer segmental dynamics and associative bond exchange dynamics to determine their influence on the relaxation of the network and on its temperature dependence. To this end, two unentangled poly(*n*-butyl acrylate) (P*n*BA) vitrimer precursors with different molar masses were synthesized through reversible addition−fragmentation chain transfer (RAFT) polymerization. Each precursor carried 10 mol % of dioxaborolane side groups. The P*n*BA backbone was chosen for its low glass transition temperature (≈219 K)[43] and its amorphous nature, which allows investigating its viscoelastic properties over a wide range of temperatures. Dioxaborolane metathesis was selected as exchange chemistry due to its catalyst-free nature and low activation energy (∼16 kJ/mol).[16] Vitrimers with different cross-linker densities were prepared by controlling the amount of cross-linker used. The Time Marching Algorithm (TMA)[44] tube model was then extended based on the linear viscoelastic data to account for the dynamics of the reversible bonds and to unravel the temperature dependence of bond exchange and segmental

https://doi.org/10.1021/acs.macromol.5c03092
Macromolecules 2026, 59, 2818−2834

Scheme 1. Synthesis of Polymer Precursor P3

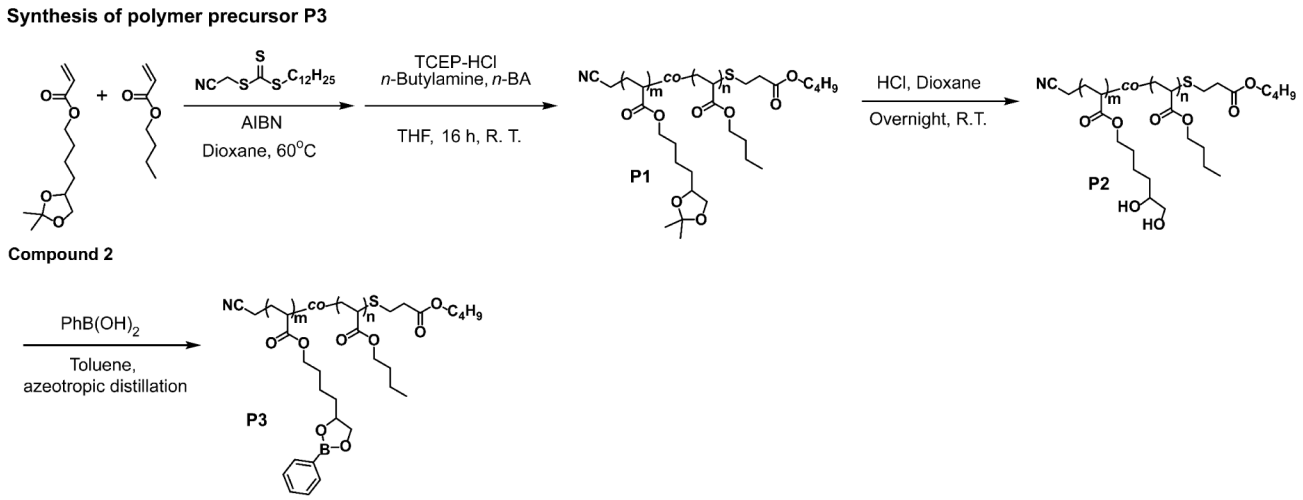

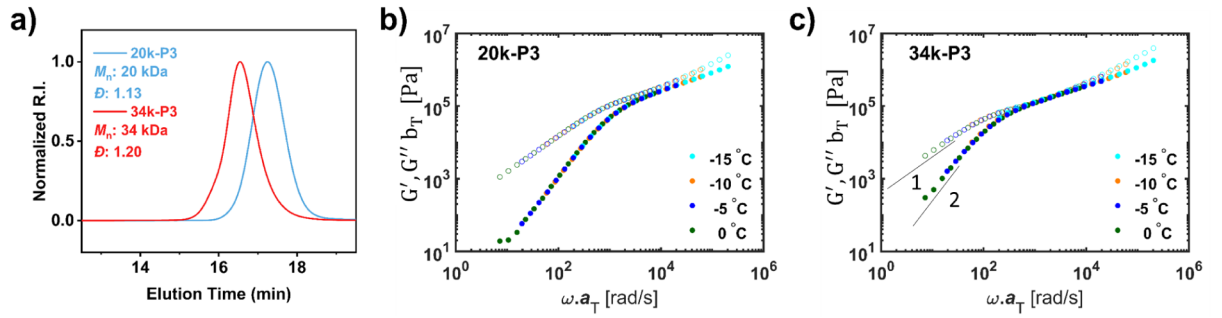

Figure 1. (a) SEC traces of the precursors, **20k-P3** and **34k-P3**, and their WLF master curves, (b) **20k-P3** and (c) **34k-P3**, with T_{ref} = 298 K, C_1 = 6.2, C_2 = 121 K.

Table 1. Structural Characteristics of the Vitrimers and Their Precursors[a]

Sample name	M_n (kg/mol)	$Đ$	DP	F	CN_f	C	$M_{xx,\ theoretical}$ (kg/mol)	T_g (°C)
20k-P3	20	1.13	140	9.6%	0	0		−41.5
20k-F10-C2					3	2%	5.0	−40.1
20k-F10-C4					6	4%	2.9	−37.5
20k-F10-C10					15	10%	1.3	−33.5
34k-P3	34	1.20	240	9.8%	0	0		−42.5
34k-F10-C2					5	2%	5.6	−39.7
34k-F10-C4					10	4%	3.1	−36.8
34k-F10-C10					25	10%	1.3	−33.4

[a]DP, the degree of polymerization F, the functionality, defined as the molar percentage of repeating units carrying a pendant dioxaborolane. CN_f, the average number of crosslinks per chain C, the mol % of crosslinks per total number of repeating units . The number average molar mass (M_n) and dispersity ($Đ$) were determined by SEC using polystyrene standards , and thus the theoretical molar mass between crosslinks (M_{xx}) was attained by dividing M_n Over CN_f + 1. The glass transition temperature (T_g) was determined by the midpoint of the glass transition step from DSC curves.

dynamics. It is worth mentioning here that the properties of vitrimers are also influenced by the type of chemical bonds and the structure of cross-linkers, though this lies beyond the scope of our current discussion. Nevertheless, we believe our conclusions can also apply to vitrimers of other nature and should enable the rational design of polymer-based vitrimers.

2. MATERIALS

2.1. Synthesis and Characterization of the Precursors

The syntheses of the functional acrylate (**Compound 2**), the bis(dioxaborolane) cross-linker (**DBX**) (Scheme S1,S2) and vitrimer precursors (Scheme 1) are adapted from our previous research.[45] Cyanomethyl dodecyl trithiocarbonate was used as the chain transfer agent (CTA) for the RAFT copolymerization of *n*BA and **Compound 2**, an acetal acrylate, (Scheme 1). To obtain copolymer precursors, **P3**, with 10% functional groups and the desired molar mass, a feed ratio of [*n*BA]:[**Compound 2**]:[CTA]:[AIBN] = 270:30.8:1:0.1 in 1,4-dioxane was used. The volume ratio of *n*BA to 1,4-dioxane was kept at 6:4. The reaction carried out at 60 °C for 9 h to achieve a number-average molar mass, M_n, of 20 kg/mol, and for 12 h to reach a M_n of 34 kg/mol (as determined by size exclusion chromatography (SEC) in *N*,*N*-dimethylformamide using a polystyrene calibration, see Figure 1a). The functionality (F) of the vitrimer precursors, which is defined as the molar percentage of repeating units carrying a pendant dioxaborolane, was measured by ^{1}H NMR. Table 1 summarizes the structural characteristics of the vitrimer precursors and vitrimers

https://doi.org/10.1021/acs.macromol.5c03092
Macromolecules 2026, 59, 2818−2834

Scheme 2. Preparation of the Vitrimers by Solution Casting[a]

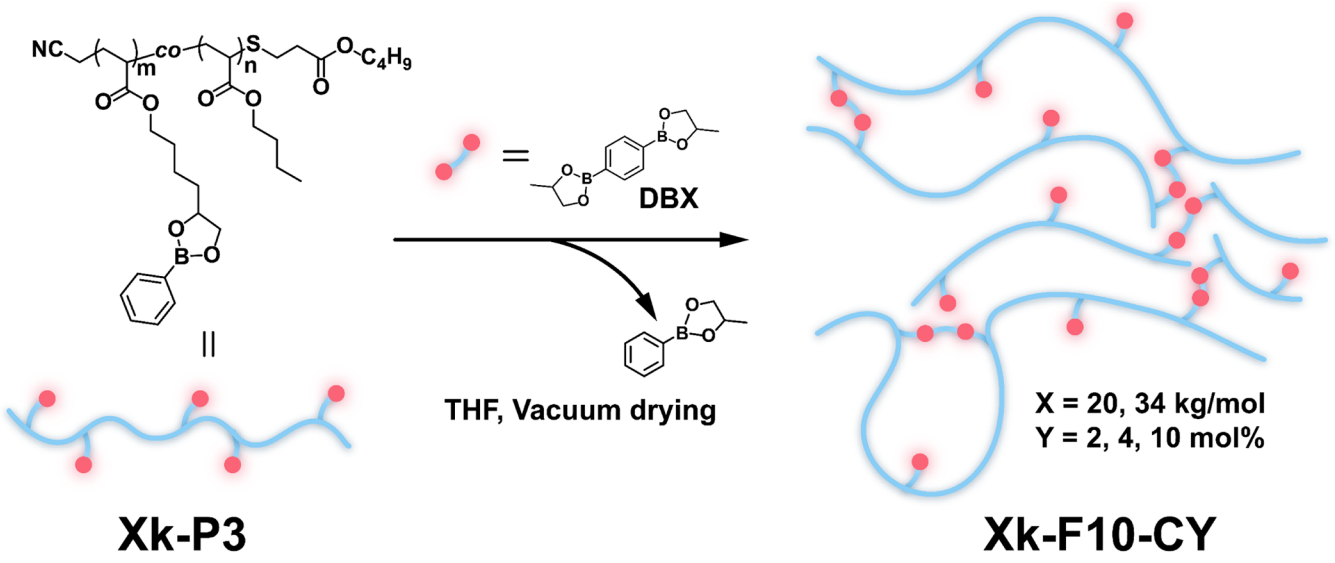

[a]X, the molar mass of the precursor (20 or 34 kg/mol); Y, the molar % of crosslinks per total number of repeating units (2, 4, or 10 mol %).

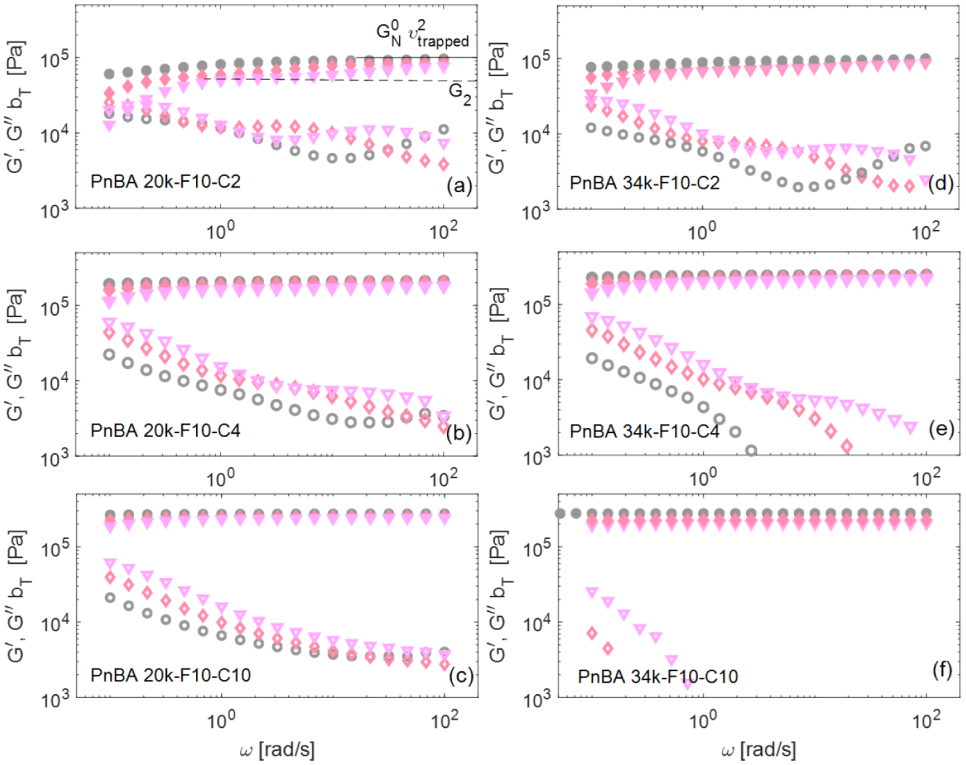

Figure 2. Frequency sweep data of 20k and 34k samples with different cross-linking degrees: C2 (a, d), C4 (b, e), and C10 (c, f), at 60 °C (o), 100 °C (◊), and 140 °C (∇). The amplitude of deformation was fixed to 5% (a), 3% (b,c,d), 1% (e) or 0.8% (f).

studied. Detailed synthesis procedures and calculations are presented in Supporting Information (SI).

2.2. Preparation of the Vitrimers Samples

Solution casting was selected for the preparation of the vitrimer networks. In a typical procedure, the polymer precursor (**P3**) was dissolved in THF (33% w/v), followed by the addition of the desired amount of cross-linker from a solution at 50 mg/mL in THF. The cross-linking density of the vitrimer network was adjusted by varying the amount of cross-linker added (Scheme 2). Three cross-linking densities (2, 4, and 10 mol %) were targeted for each vitrimer precursor (20k-P3 and 34k-P3), yielding six distinct vitrimers in total (Table 1 and SI). During the cross-linking process, the pendent dioxaborolane functions of X-P3 react with the cross-linker **DBX** to form cross-linking points, generating 4-methyl-2-phenyl-1,3,2-dioxaborolane (b.p.: 54−56 °C at 0.5 mm Hg) as a byproduct.[46] To remove the residual solvent and the byproducts, the gel-like samples were first left under ambient atmosphere overnight to allow partial solvent evaporation, followed by vacuum drying at 80 °C for 2 weeks.[24,47] The resulting material was broken into small pieces and reshaped using a hot press for the rheological measurements (see SI). The glass transition temperatures, T_g, were measured by differential

https://doi.org/10.1021/acs.macromol.5c03092
Macromolecules 2026, 59, 2818−2834

scanning calorimetry (DSC) and are summarized in Table 1 The results showed an increase in T_g with increasing cross-linking density.

3. VISCOELASTIC RESPONSE OF THE VITRIMERS

3.1. Linear Viscoelastic Data (LVE)

3.1.1. LVE of the Precursor. The small-amplitude oscillatory shear (SAOS) response of the vitrimer precursors **20k-P3** and **34k-P3** (see Table 1) was measured using an ARES rheometer (TA Instruments) with 8 mm parallel plate geometry, at temperatures ranging from −15 to 0 °C, with frequencies ranging from 100 rad/s to 0.1 rad/s, and with a strain amplitude fixed to 5% to ensure being in the linear regime of deformation. The corresponding master curves were then constructed according to the WLF equation (eq 1),[22]

$$\log a_T = \frac{-C_1(T - T_{ref})}{C_2 + T - T_{ref}} \quad (1)$$

with T_{ref} = 298 K, C_1 = 6.2, C_2 = 121 K (Figure 1b,c). A small vertical shift b_T has also been applied to account for the density correction, similar to refs.[48,49] The viscoelastic response of **20k-P3** and **34k-P3** corresponds to the response expected for unentangled or very poorly entangled polymers. This is normal as P*n*BA chains have an average molar mass between two entanglements of around 18 kg/mol.[6,50] For both samples, the slopes of G' and G'' in the terminal region are very close to slopes 2 and 1 observed for a fully relaxed sample.

3.1.2. LVE of the Vitrimers: Influence of the Cross-Linking Density and of the Molar Mass. Then, SAOS measurements of vitrimer samples were conducted from 180 °C to −20 °C, with frequencies ranging from 100 rad/s to 0.03 rad/s. For each system, the strain amplitude was fixed to ensure to be in the linear regime of deformation. Before their measurements, the samples were equilibrated in the rheometer at 180 °C during 120 min. The reproducibility of the data was checked for all systems. Main results are shown in Figure 2, for representative temperatures.

All the samples present a clear and well-defined elastic plateau, attributed to the chain cross-linking. As also shown in Figure 3a,b, the plateau modulus (G_N^0) rises with the cross-linking density. For C2 and C4 samples, its value is found to be slightly lower than the one estimated by the phantom model corrected to account for the presence of dangling ends (see SI, Table S2), while for the C10 vitrimers, it is much lower than its theoretical value, suggesting the presence of a higher proportion of elastically ineffective cross-links (e.g., loops).[51] It must be noted that the Phantom model accounts for possible fluctuations of the branching points, which cannot be considered in tube models. It is also observed that the signal of G'' is lost with sample **34k-F10-C10** (see Figure 2f) and partly lost with sample **34k-F10-C4** (see Figure 2e). This unusual result can be explained by the large density of cross-linked functional groups of this sample, leading to the presence of a low fraction of dangling chains. Consequently, between the relaxation of these dangling ends and the time at which the bond exchange start of occur, the response of the sample is fully elastic.[52] For the vitrimer samples with lower degrees of cross-linking, this loss of G'' data is not observed and the storage modulus curve displays two elastic plateau, G_N^0 (or slightly less (i.e.,$G_N^0 \upsilon_{trapped}^2$) if the relaxation of the dangling ends is accounted for, see Section 3.2.3) and G_2 (with $G_N^0 \geq G_2$), as well as two relaxation peaks in G, which are especially

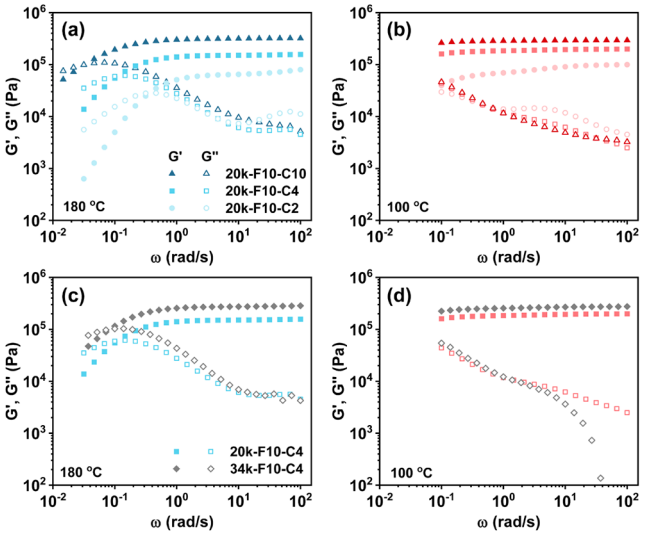

Figure 3. Influence of the cross-linking density: The storage and loss moduli of **20k-P3** based vitrimers with varied cross-linking density are compared, at T = 180 °C (a) or 100 °C (b). Influence of the molar mass of the precursor: The storage and loss moduli of **20k-F10-C4** and **34k-F10-C4** vitrimers are compared, at T =180 °C (c) or 100 °C (d).

visible for samples **20k-F10-C2** and **34k-F10-C2** at 140 °C. The faster relaxation process, which takes place at intermediate frequencies and describes the transition of G' from $G_N^0 \upsilon_{trapped}^2$ to G_2, is barely visible for longer chains (Figure 2a vs Figure 2d) or samples with a larger proportion of cross-linkers (C10). This transition may have several origins, such as the presence of dangling ends, the partial relaxation of the network due to local exchange processes, or the presence of complex assemblies made of several chains but not fully trapped in the network. This is investigated in Section 3.2. The slower relaxation process is attributed to the chain motion and network relaxation via dioxaborolane exchange mechanism. The terminal relaxation process is nearly absent at 60 °C (being too slow to be measured), while it clearly takes place above 100 °C. It also depends on the density of cross-linkers (Figure 3) and on the molar mass of the precursor. As investigated in Section 3.2, this could be due to either the influence of sample composition on the lifetime of the dynamic dioxaborolane cross-links, or to a cooperative effect of the dynamic bonds along the same precursor chain. We note, however, that the loss modulus peaks of the different samples superimpose when this relaxation process starts (i.e., on the high frequency side of the peaks, at around ω = 1 rad/s), independently of the cross-linker density (Figure 3a,b) and of the molar mass (Figure 3c,d), until the maximum of the G'' peak is reached. This suggests that the sticker exchange dynamics start at the same time for all these systems and progress in a similar way, as long as it takes place on a length scale smaller than the length scale of the whole chains.

3.1.3. LVE of the Vitrimers: Influence of the Temperature. To determine the influence of temperature on the viscoelastic properties of these vitrimers, we then try to build their (pseudo)master curves. At low temperatures, at which the exchange dynamics of the cross-linkers is too slow to be measured, the dynamics of the network is governed by the segmental dynamics of the chains which compose the network, and is therefore expected to follow a WLF equation.[22,53]

https://doi.org/10.1021/acs.macromol.5c03092
Macromolecules 2026, 59, 2818−2834

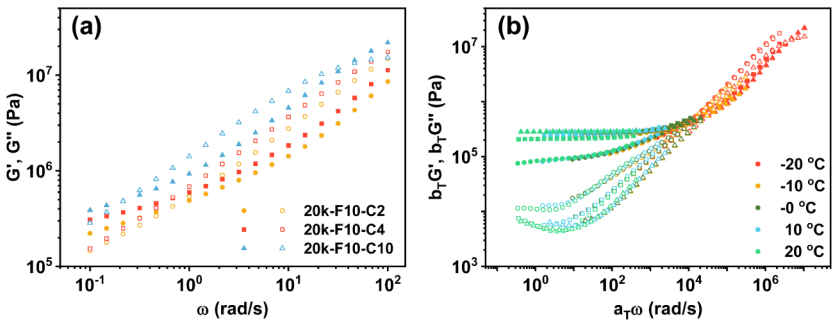

Figure 4. (a) Frequency sweep data at −20 °C for the vitrimers samples based on the precursor **20k-P3** and a cross-linker degree of 10% (blue triangles (**20k-F10-C10**)), 4% (brown circles (**20k-F10-C4**)), and 2% (red squares (**20k-F10-C2**)); (b) Comparison of WLF shifted master curves of the foregoing vitrimers built from the **20k-P3** precursor, at temperatures range from −20 to 20 °C. The data have been shifted, based on eq 2.

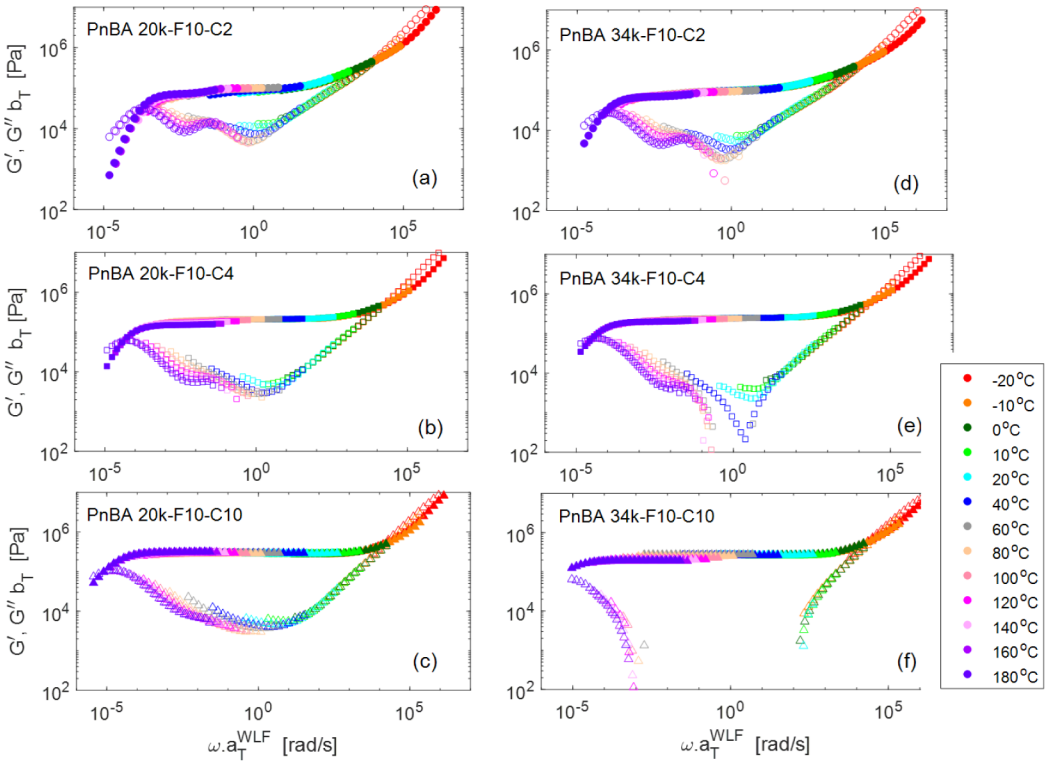

Figure 5. Storage and loss moduli of the vitrimer samples measured at temperatures ranging from −20 to 180 °C, and shifted into pseudomaster curves, based on the WLF horizontal shift factors determined from eq 2 The universal constants C_1 = 6.2 and C_2 = 121 K are used for all samples.

However, since the cross-linking degree influences the glass transition temperature (see Table 1), the data of the different vitrimers cannot be directly compared at a specific temperature. This is illustrated in Figure 4a., where it is seen that at −20 °C, the linear viscoelastic response of the vitrimer samples do not superimpose at high frequency.

To account for this difference in T_g, the shift factors are calculated using the same WLF parameters C_1 and C_2 as for the precursors, but based on another reference temperature, T_{ref}^{WLF}, to ensure that this temperature fulfils *iso*-friction condition, fixed here as $T_{ref}^{WLF} = T_g + 68$ °C. Finally, these master curves are shifted to the reference temperature T_{ref} = 30 °C, which is far enough from T_g to ensure the good overlap of the curves in the high frequency regime, where the local dynamics does not depend on the cross-linking density:

$$\log a_T = \frac{-C_1(T - T_{ref}^{WLF})}{C_2 + T - T_{ref}^{WLF}} \cdot \left(\frac{-C_1(30 - T_{ref}^{WLF})}{C_2 + 30 - T_{ref}^{WLF}}\right)^{-1} = \log a_T^{WLF} - \log a_T^{WLF}(30\ ^\circ\mathrm{C}) \quad (2)$$

Vertical shift factors are also applied, to account for the temperature dependence of the density of P*n*BA.[54] As shown in Figure 4b, the storage and loss moduli of the master curves obtained for the different samples superimpose well below 20 °C. This confirms that at these low temperatures and short time scales, the network behaves similarly as a stable network, either because the dynamic bond exchanges are hindered at these low temperatures ($T < T_v$), or because they are too slow to be measured.[14]

Figure 5 presents the master curves of the vitrimers with different amounts of cross-linker, based on the WLF eq 2, but considering temperatures ranging from −20 to 180 °C. Except for sample **34k-F10-C10**, a crossover between the storage and

https://doi.org/10.1021/acs.macromol.5c03092
Macromolecules 2026, 59, 2818−2834

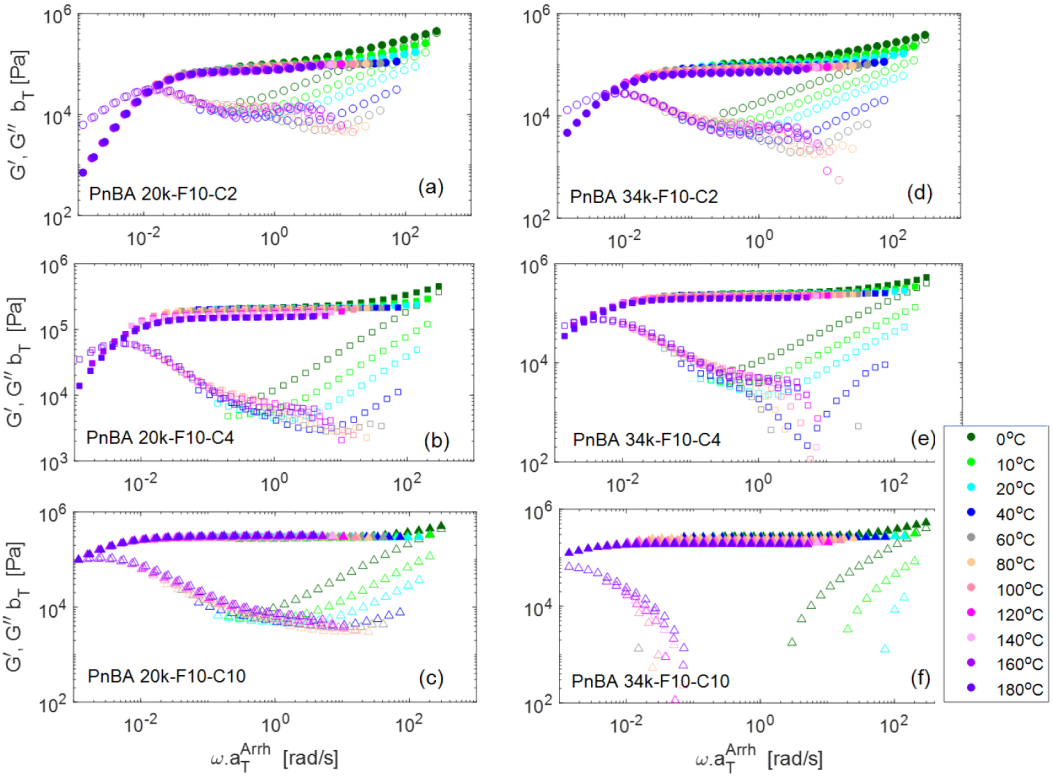

Figure 6. Storage and loss moduli of the vitrimer samples measured at temperatures ranging from −20 to 180 °C, and shifted into master curves, based on the horizontal shift factors a_T^{Arrh} determined from an Arrhenius equation and considering E_a = 25 kJ/mol.

loss moduli is observed at low frequency, indicating that the vitrimer chains are able to (partially) relax due to the exchangeable nature of dynamic chemical cross-links.

Above 20 °C, for all vitrimers samples, the curves fail to superimpose based on a WLF shift, leading to a thermo-rheological complex behavior beyond simple chain motion. Such a complexity was expected since with the increase of temperature, the dynamics of the network is governed by the bond exchange process, which is known to follow an Arrhenius dependence rather than a WLF dependence.[3,55−57] This is shown in Figure 6, where Arrhenius shift factors were applied to all the data, with an activation energy, E_a which has been fixed such as a good overlap of the low frequency data is obtained, since it is in this regime that the bonds exchange process dominates:

$$\log(a_T^{Arrh}) = \frac{E_a}{R}\left(\frac{1}{T} - \frac{1}{T_{ref}}\right) \quad (3)$$

While these Arrhenius shifts are not acceptable at low temperatures ($T \leq 30$ °C), at which the network topology remains relatively stable (see Figure 4b), both the G' and G'' superimpose well at high temperatures (≥60 °C) and at low frequency, if an activation energy of 25 kJ/mol is considered.

This value is slightly higher than the activation energy for the exchange reaction between small molecules, which has been evaluated to 16 kJ/mol in a previous work.[58] For associative-type bonds like dioxaborolanes, there is no intermediate state in which the cross-linked dioxaborolane separates into two parts; rather, a successful exchange requires initial contact, alignment, and then exchange. It is consequently reasonable to consider the process as a single-step reaction with Arrhenius-type behavior. However, the motion of these pendent or cross-linked dynamic bonds is less free than that of small molecules, as they are attached to the backbone of a chain. This may result in slightly higher activation energy compared to that in small-molecule models. In previous works, even higher activation energy (40 to 80 kJ/mol) has been found for vitrimers based on dioxaborolane bond exchange, with poly(methyl methacrylate) or poly(hexyl methacrylate) backbone,[16,24] while an activation energy of 33 ± 4 kJ/mol has been found for polybutadiene vitrimers.[59] We attribute these different values of E_a to the fact that apparent activation energy of the networks contain two contributions: one from the dioxaborolane bond exchange, and another one from the polymer chain dynamics, the influence of the latter being more important for precursors with a higher glass transition temperature.[60]

On Figure 6, it is also observed that the same activation energy has been used for all samples, independently of their cross-linking density and of the molar mass of the precursor, which suggests that the temperature dependence of the bond exchange process does not vary with these two parameters.

Thus, by combining WLF shift factors at low temperatures and Arrhenius shift factors at high temperatures, it is possible to build pseudomaster curves, considering the whole range of temperatures. It must be noted however that this shifting method differs from the one usually used for supramolecular systems, which combines WLF and Arrhenius shifts at low frequency, considering that the terminal regime is affected by both dynamics (i.e., $a_T = a_T^{WLF}.a_T^{Arrh}$). Indeed, it can be seen in Figure 5 that applying WLF shifts to high temperature data leads to a terminal relaxation process which is slower for the high temperature data than for the lower temperature data. Consequently, multiplying WLF and Arrhenius shift factors

https://doi.org/10.1021/acs.macromol.5c03092
Macromolecules 2026, 59, 2818−2834

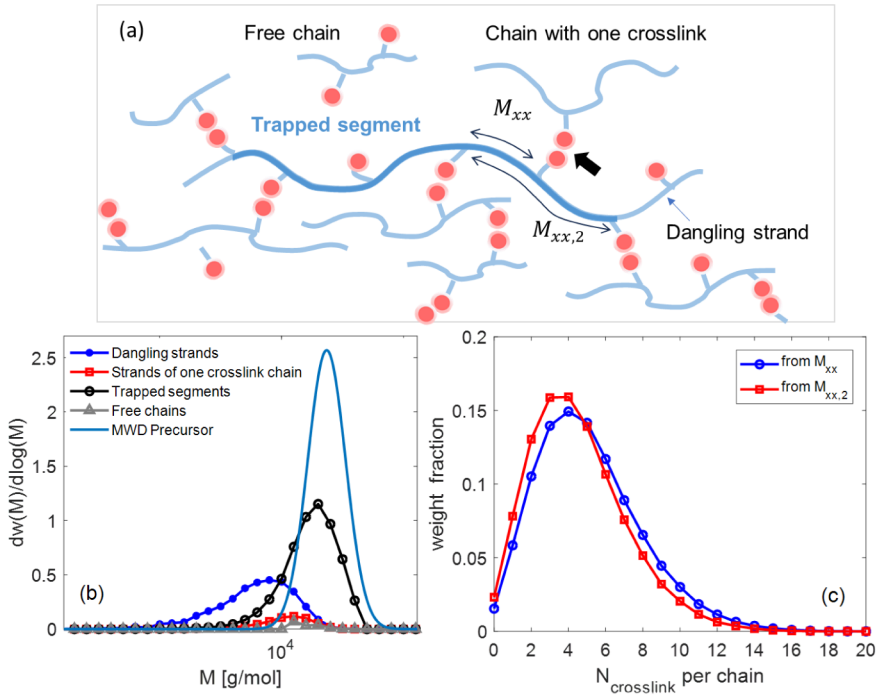

Figure 7. (a) Cartoon representing the cross-linked strands in a vitrimer network, and the different types of molecular segments. There are 1) the free chains, which do not contain effective cross-link, 2) the dangling arms belonging to a chain with only one cross-linking point, 3) the dangling strands, which belongs to chains with at least two effective cross-links, and 4) the trapped segments, which are the molecular segments trapped between the first and the last cross-linking points of a chain. The black arrow shows a cross-link, which is assumed not to contribute to the low frequency plateau. (b) Molar mass distributions of the different types of molecular segments. (c) The weight fraction of vitrimer chains as a function of the number of cross-links they contain, considering all cross-linking points or only the ones participating to the second (low frequency) plateau. The results have been determined by considering the MWD of the precursor 20k-P3 and M_{xx} = 4320 g/mol and $M_{xx,2}$ = 4860 g/mol, which corresponds to sample 20k-F10-C4.

would imply using a negative activation energy to compensate this too strong effect of the WLF shift factors, which does not make sense. Similar observation was already made in literature, in ref 57.

At intermediate frequency, i.e., in the frequency window from 10^{-2} to 10 rad/s, both the WLF and Arrhenius shifts fail to construct an acceptable master curve of these vitrimers. Thermo-rheological complexity is still observed, suggesting that the temperature dependence of the corresponding intermediate process involves both dynamics, which cannot be easily separated. In the next section, we analyze the data with a tube-based model, to understand the influence of temperature on this intermediate process.

3.2. Modeling the Linear Viscoelastic Properties

To further analyze the data, we modify our time marching algorithm model (TMA) to account for the different relaxation processes observed experimentally. This requires, first, to describe the statistical composition of the vitrimer networks based on the probability for a monomer to be a functional group cross-linked to another chain. More specifically, we need to determine the proportions and molar masses of the dangling ends, and the molecular segments trapped between the cross-linking points. We also need to know the average number of cross-links per chain. This composition is then used to determine the corresponding G' and G'' curves and compare them to experimental data. As it will be discussed in Section 3.3, this approach is based on some unknown parameters. First, their values are fixed by best-fitting procedure, and in a second step, these best-fit values are analyzed to elucidate the interactions between polymer segments and dynamic cross-linking interactions, and to discuss the influence of temperature, cross-linking density and molar mass of the chains on the exchange dynamics of the cross-linkers.

3.2.1. Statistical Composition of a Vitrimers Sample.

A statistical approach is first developed to describe the samples composition. To predict their corresponding viscoelastic properties, one needs to determine the proportion and molar mass of the free chains, dangling ends and molecular segments trapped between two cross-linking points. The input data are the molar mass distribution of the precursor as well as the probability p_x for a monomer along the chain backbone to be a functional group cross-linked to another chain. This probability is considered as a fit parameter. As already mentioned, at low cross-linking density (C2 and C4), two rubbery plateaus are observed (see Figure 2a). As shown in Section 3.2.3, the transition between these two plateaus cannot be attributed to the relaxation of the dangling ends, the latter relaxing at higher frequency (shorter time). Therefore, to model this transition, we consider the existence of two different mesh sizes in the network or, equivalently, to the existence of two types of cross-links characterized by different lifetimes. While the probability for a monomer to be a cross-linking point is equal to p_x, the probability for a monomer to be a cross-linking point that contributes to the second (low frequency) elastic plateau is assumed to be equal to $p_{x,2}$. As illustrated in Figure 7a, the corresponding number-average molar masses between two effective cross-linkers, M_{xx} and $M_{xx,2}$ are:

$$M_{xx} = m_0 / p_x \tag{4}$$

https://doi.org/10.1021/acs.macromol.5c03092
Macromolecules 2026, 59, 2818−2834

$$M_{xx,2} = m_0 / p_{x,2} \quad (5)$$

with m_0, the molar mass of a monomer.

Assuming that p_x and $p_{x,2}$ are known, for each molar mass M_i, a large ensemble of chains is then created (around 1000 chains are needed) and cross-linking groups are randomly placed along their backbone. Following ref.,[50] the molecular segments are then sorted into free chains (i.e., with no effective cross-link), chains containing only one effective cross-link, dangling arms and molecular segments trapped between the first and the last cross-linking junctions (see Figure 7a) and their corresponding molar mass distributions are determined (see Figure 7b). The latter are then rescaled, to account for the fact that the chains of mass M_i represent a weight fraction υ_i of the sample, which is determined from its molecular weight distribution (MWD).

3.2.2. LVE of the Precursors. We first model the linear viscoelastic data of the precursors. This allows us to determine their corresponding Rouse time at the reference temperature T_{ref} of 30 °C. Since the molar mass between two entanglements, M_e, is around 18 kg/mol for P*n*BA, we can assume that the two precursors **20k-P3** and **34k-P3** are unentangled. Consequently, their relaxation modulus $G(t)$ should be well approximated by the Rouse model:

$$G(t) = \sum_i \upsilon_i G_i(t) \quad (6)$$

$$G_i(t) = \frac{\rho RT}{M_i} \sum_{p=1}^{N_i} \exp\left(-\frac{2p^2 t}{\tau_R(M_i)}\right) \quad (7)$$

where N_i is the number of Kuhn segments in the chain of mass M_i, ρ is the density, R is the ideal gas constant, and $\tau_R(M_i)$ is the Rouse relaxation time of the whole chain. The storage and loss moduli are then obtained from $G(t)$ based on the Schwarzl functions.[61] The theoretical curves are compared to the experimental data in Figure 8. A good agreement is obtained based on $\tau_R(M) = \tau_e(\frac{M}{M_e})^2$, with τ_e being the Rouse time of a strand of mass M_e = 18 kg/mol. Its value has been fixed to 0.0015 *s* at a reference temperature of 30 °C. In eq 7, the product ρRT has been fixed to $\frac{5}{4}G^0_{N,ent}M_e$, with $G^0_{N,ent} = 160\ kPa$, in order to keep consistency with previous works on entangled P*n*BA polymers.[48] The molar mass dispersity of the sample has been accounted for by considering log-normal distribution for the molar mass distribution, with a dispersity of 1.2 and 1.25 for samples **20k-P3** and **34k-P3**, respectively.

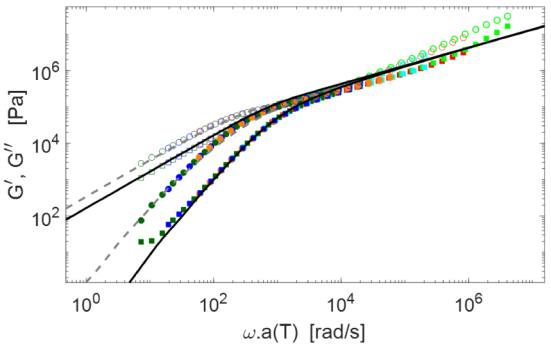

Figure 8. Storage and Loss moduli of the precursors, **20k-P3** (□) and **34k-P3** at 30 °C (o). Comparison between the experimental data and the predictions (continuous and dashed curves for samples **20k-P3** and **34k-P3**, respectively) obtained with the Rouse eq7.

3.2.3. LVE of the Vitrimers. As described in Table 1, the cross-linking density of the vitrimer networks is quite high (with M_{xx} ranging from 1.3 kg/mol to 5 kg/mol). Consequently, at a time shorter than the exchange lifetime of the cross-links, the mesh-size of the network is much smaller than the length of the chains (20 kg/mol or 34 kg/mol), and entanglements or, at least temporary chain interactions, must be accounted for in the modeling. Indeed, it is expected that an uncross-linked (free) chain will not be able to relax by a Rouse process, as it is constrained by the dynamic network through which it has to diffuse (reptate) to renew its configuration. Moreover, since the average molar mass between two entanglements, M_e, is equal to 18 kg/mol for P*n*BA, any assembly built from the association of two or more precursor chains is expected to be entangled. Therefore, both the cross-linking junctions and the possible entanglements/interactions between the interpenetrated chains are expected to influence the dynamics of the chain segments and must be considered to model the relaxation of the free chains and dangling ends. Following ref 62, we define the corresponding average molar mass, $M_{xx,e}$, between two topological constraints as:

$$M_{xx,e} = \left(\frac{1}{M_{xx}} + \frac{1}{M_e}\right)^{-1} \quad (8)$$

Same Equation applies in case of $M_{xx,2}$, leading to $M_{xx,e,2}$. Since $M_{xx} < M_e$, the contribution of the entanglements stays, however, limited. The corresponding plateau modulus is equal to $G^0_N = \frac{4\rho RT}{5M_{xx,e}} = G^0_{N,ent}\frac{M_e}{M_{xx,e}}$, with $G^0_{N,ent} = 160\ kPa$. This value is then used to determine the relaxation modulus $G(t)$ of the vitrimers:

$$G(t) = G_R(t) + G^0_N \cdot \left(\upsilon_{dang}\varphi_{dang}(t)\Phi_{CR}(t) + \upsilon_{trapped}\Phi_{CR}(t)\phi_{interm}(t)\phi_{crosslinks}(t)\right) \quad (9)$$

The first contribution, $G_R(t)$, accounts for the high frequency Rouse relaxation of the molecular segments between two cross-linkers/entanglements:

$$G_R(t) = \frac{\rho RT}{M_{xx,e}} \sum_{p=1}^{N_{xx,e}} \exp\left(-\frac{2p^2 t}{\tau_{xx,e}}\right) \quad (10)$$

with $N_{xx,e} = \frac{M_{xx,e}}{m_0}$, the number of Kuhn segments in a molecular strand of mass $M_{xx,e}$, and $\tau_{xx,e} = \tau_R(M_{xx,e}) = \tau_e(\frac{M_{xx,e}}{M_e})^2$, their corresponding Rouse time. The parameter υ_{dang} is the weight fraction of dangling chains (free chains, chains with one cross-linking point, or any dangling ends) while $\upsilon_{trapped} = (1 - \upsilon_{dang})$is the weight fraction of molecular segments trapped between two cross-linking junctions. The first term in the parentheses, $\upsilon_{dang}\varphi_{dang}(t)$-$\Phi_{CR}(t)$, describes the contribution of the free chains and dangling ends to the relaxation modulus. The function $\varphi_{dang}(t)$ represents the probability that a molecular segment belonging to a dangling chain is not relaxed at time *t*, while accounting for its possible relaxation by Contour Length Fluctuations (CLF) and by reptation (in the case of the free linear chains):

https://doi.org/10.1021/acs.macromol.5c03092
Macromolecules 2026, 59, 2818−2834

$$\varphi_{dang}(t) = \frac{1}{\upsilon_{dang}}\left[\sum_{i,dang} \upsilon_{i,dang}\varphi_{i,dang}(t) + \sum_{i,lin} \upsilon_{i,lin}\varphi_{i,lin}(t)\right] \quad (11)$$

$$\varphi_{i,dang}(t) = \sum_{x=1/100}^{x=100/100} \exp\left(-\frac{t}{\tau_{fluc}(x, M_i)}\right)\Delta x \quad (12)$$

$$\varphi_{i,lin}(t) = \sum_{x=1/100}^{x=100/100} \exp\left(-\frac{t}{\tau_{fluc}(x, M_i)}\right)\exp\left(-\frac{t}{\tau_{rept}(x, M_i)}\right)\Delta x \quad (13)$$

with $\upsilon_{i,dang}$ and $\upsilon_{i,lin}$, the weight fractions of dangling chains of mass M_i and of linear chains (free of cross-linkers) of mass M_i, which are determined from the statistical composition of the vitrimer (see Section 3.2.1). The survival probability $\varphi_{i,dang}(t)$ of a dangling arm i is determined by summing the survival probabilities of all its molecular segments x (from $x = 0$ at the chain extremity to $x = 1$ in the middle of the chains or at the branching point, with $\Delta x = 1/100$), while considering that they can relax by CLF. Similar approach is applied to the free linear chains, which can also relax by reptation, in addition to CLF. The determination of their corresponding fluctuation times $\tau_{fluc}(x,M_i)$ and reptation time $\tau_{rept}(x,M_i)$ is detailed in ref 62. The function $\Phi_{CR}(t)$ accounts for the Constraint Release process coming from the motions of the dangling arms and free chains within the network. Since this process takes place before the exchange dynamics of the cross-links is becoming active, $\Phi_{CR}(t) = \upsilon_{trapped} + \varphi_{dang}(t)$, going from 1 at short times to $\upsilon_{trapped}$ after the relaxation of the dangling chains.

The second term in eq 9, $\upsilon_{trapped}\Phi_{CR}(t)\phi_{interm}(t)\phi_{crosslinks}(t)$, is related to the relaxation of the vitrimer network. After the constraint release effect from the relaxed dangling arms, the remaining topological constraints are attributed to the cross-linking junctions. As discussed above, a small fraction of the latter may relax at intermediate times, before the relaxation of the other topological constraints via the cross-link exchange dynamics. As further discussed in Section 3.3, we attribute this faster relaxation to the relaxation of molecular segments located between two branching points but poorly trapped in the network, thus able to relax even if the exchange dynamics is not yet activated. It should describe the transition of the network, from a mesh-size M_{xx} to a mesh-size $M_{xx,2}$, i.e., from a rubbery plateau $G_N^0\upsilon_{trapped}^2$ reached just after the relaxation of the dangling arms to a rubbery plateau equal to $G_2 = G_N^0\left(\frac{M_{xx,e}}{M_{xx,e,2}}\right)\upsilon_{trapped}^2$ just after this intermediate relaxation. Therefore, assuming that the characteristic time of this relaxation process is τ_{br}, we describe it as:

$$\phi_{interm}(t) = \left(\frac{M_{xx,e}}{M_{xx,e,2}}\right) + \left(1 - \frac{M_{xx,e}}{M_{xx,e,2}}\right)\exp\left(-\frac{p^2 t}{\tau_{br}}\right) \quad (14)$$

The influence of this intermediate process is mainly observed for the samples containing a low density of cross-linkers (C2 and C4).

Finally, the function $\phi_{crosslinks}(t)$ corresponds to the relaxation status of the network through the dynamics of exchange of the dynamic bonds. To effectively relax, cross-linking points must encounter each other multiple times before successfully swapping partners.[63] The corresponding lifetime of this process is called $\tau_{exchange}$, while the number of cross-links (also called "stickers") per chain is N_{st}. Since the network is becoming dynamic, and since the chains are not entangled, their relaxation is well described by a sticky Rouse process.[3] The characteristic sticky Rouse relaxation time of the whole chain is equal to $\tau_{exchange}N_{st}^2$. Accounting for the different modes p of relaxation, $\phi_{crosslinks}$ is thus described as:[40]

$$\phi_{crosslinks}(t) = \sum_{st} \upsilon_{st}\left(\frac{1}{N_{st}}\sum_{p=1}^{N_{st}} \exp\left(-\frac{p^2 t}{\tau_{exchange}N_{st}^2}\right)\right) \quad (15)$$

where υ_{st} is the proportion of chains containing N_{st} stickers. Its value is determined from the statistical composition of the network (see Section 3.2.1). The $G(t)$ is then converted into the dynamic modulus curves via the approximation functions of Schwarzl.[61]

This model is based on a series of parameters. First, there are the three parameters related to the tube model, $G_{N,ent}^0$, M_e and τ_e (30 °C). These values are known from previous studies, and are fixed to 160 kPa, 18 kg/mol and 0.0015 s, respectively. They have been successfully used for predicting the viscoelastic properties of the precursors. Then, one needs to determine M_{xx}, $M_{xx,2}$the exchange lifetime $\tau_{exchange,30\ °C}$ of the junctions at 30 °C, as well as the relaxation time of the intermediate process, $\tau_{br,30\ °C}$, at 30 °C. These parameters, which are first taken as fit parameters, are analyzed in Section 3.3. But before discussing these values, we investigate, in the next section, the influence of temperature on these parameters.

3.2.4. Influence of Temperature on the LVE of the Vitrimers. The linear viscoelastic properties of the vitrimers show thermo-rheological complexity. Therefore, to avoid wrong interpretation due to the shifting of the data into a pseudomaster curve, we model the data at each temperature T separately, and account for the influence of temperature directly on the model parameters τ_e, $\tau_{exchange}$ and τ_{br}.

The temperature effect on the segmental dynamics is accounted for by rescaling the Rouse relaxation time τ_e of a molecular segment of mass M_e = 18 kg/mol:

$$\tau_e = \tau_e\,(30°C)\,a_T \quad (16)$$

with a_T described by eq 2. On the other side, the exchange lifetime of a sticker must follow an Arrhenius dependence. As the temperature increases, cross-linked dioxaborolanes are more frequently engaged in exchange reactions, driven by the accelerated chain motion that leads to more frequent collisions. Therefore, the time needed for an effective collision that enables a successful partner exchange decreases. We thus assume that $\tau_{exchange}$ is well approximated by:

$$\tau_{exchange} = \tau_{exchange,30\ °C}\exp\left(\frac{E_a}{R}\left(\frac{1}{T} - \frac{1}{303.15}\right)\right) \quad (17)$$

From the analysis of the experimental data, we fixed the activation energy for flow, E_a, to 25 kJ/mol.

As already mentioned, the temperature dependence of the intermediate relaxation process is not clear. Therefore, as a first approach, we model the viscoelastic data of the representative sample 20K-F10-C4, while considering τ_{br} (eq 14) as a fit parameter for each different temperature. The two mesh sizes are fixed by best-fitting, to well describe the level of the two plateaus and the terminal regime. Their values are M_{xx} = 4320 g/mol, $M_{xx,2}$ = 4860 g/mol and $\tau_{exchange,30\ °C}$ = 81 s (see Section

https://doi.org/10.1021/acs.macromol.5c03092
Macromolecules 2026, 59, 2818−2834

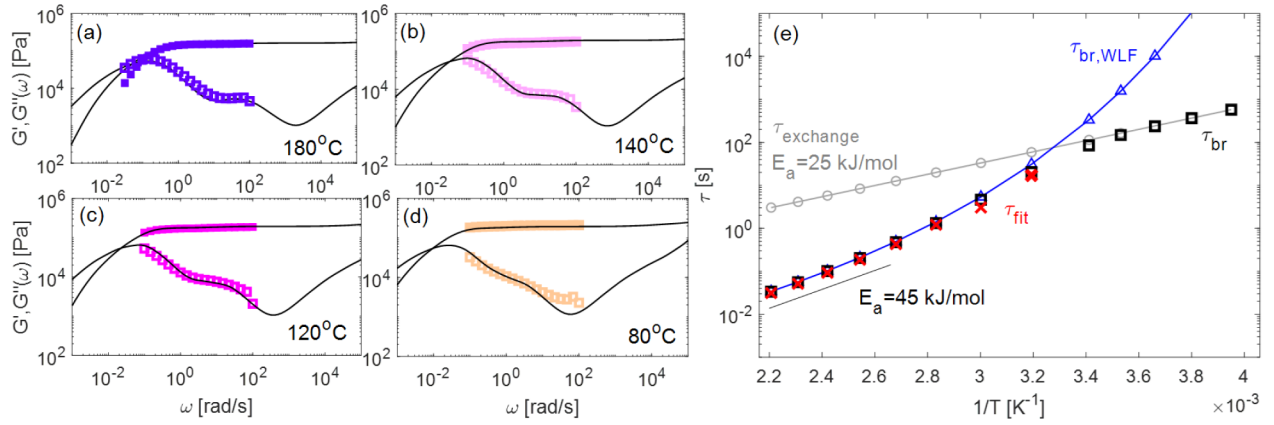

Figure 9. Comparison between experimental storage (filled symbols) and loss (empty symbols) moduli of 20k-F10-C4 sample and their theoretical description (continuous curves) at (a) 180 °C, (b) 140 °C, (c) 120 °C and (d) 80 °C. (e): Comparison between the value of τ_{br} obtained by best-fitting (called τ_{fit} see the red x), $\tau_{exchange}$ (eq 17, gray o) and $\tau_{br,WLF}$ with $\tau_{br,WLF}$ (30 °C) = 92 s (eq 19, blue Δ), as a function of $1/T$. The black squared symbols represent the results obtained for τ_{br} with eq 18 and considering that $\tau_{br,WLF}$ (30 °C) = 92 s.

3.3). The results obtained are shown in Figure 9a−d, for the representative temperatures of 80, 120, 140, and 180 °C. The experimental data are well described by the model at high and low frequencies, which confirms that the influence of temperature is correctly accounted for by eqs 16 and 17. The best-fit values taken for τ_{br} are shown in Figure 9e (see the red crosses), in function of the inverse absolute temperature.

Interestingly, at high temperatures ($T \geq 80$ °C), these relaxation times exhibit a WLF dependence on temperature (also well approximated by an Arrhenius dependence with an activation energy E_a = 45 kJ/mol), with $\tau_{br,WLF}$ (30 °C) fixed to 92 s. This suggests that in this range of temperature, the intermediate relaxation process is primarily driven by segmental motions and not by the exchange dynamics. From this observation, and knowing that the intermediate relaxation process is mainly visible for the loosely connected networks **34k-F10-C2**, **20k-F10-C2** and **20k-F10-C4**, we attribute this process to the presence of a small fraction of cross-links which are not fully trapped within the network. Such cross-links involve, for example, a chain with only one cross-linking junction. As illustrated in Figure 10, these loosely connected cross-linking points can move at the rhythm of the fluctuation process of the branches attached,[64] allowing the relaxation of molecular segments on a length scale larger than $M_{e,xx}$. This process, which takes place even if the cross-linking junctions are considered as permanent, is governed by the segmental dynamics.

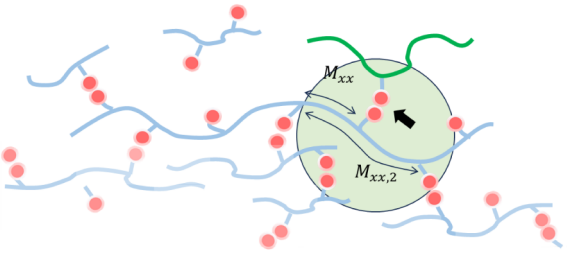

Figure 10. Illustration of the loosely connected cross-linking points, shown by the black arrow. The light green circle represents a subchain able to disorient and relax before the bond exchange process takes place. Its relaxation requires the motion of the dangling branches attached to the loosely connected cross-linking points (represented in green).

However, as shown in Figure 5, a significant deviation from a WLF T-dependence occurs at temperatures below 60 °C, at which the intermediate relaxation process is speeded up compared to a relaxation process only governed by the segmental dynamics. In fact, one can see in Figure 9e that in this range of temperatures, the exchange bond time $\tau_{exchange}$ becomes faster than the time $\tau_{br,WLF}$ needed for a segment of mass $M_{xx,2}$ to relax while considering the network as permanent. Indeed, at these low temperatures, due to the greater temperature dependence of the WLF process, the motion of the cross-linking points triggered by the fluctuations of the dangling branches is becoming very slow, much slower than their motion due to the exchange dynamics. Consequently, the latter process is becoming dominant.

The thermo-rheological behavior observed in this regime is thus attributed to the evolution of the relative importance of these two relaxation processes (motion of the loosely connected cross-linking points due to the motion of the dangling ends attached, versus relaxation of the loosely connected cross-linking points due to the bond exchange process) with temperature, which originates from their different dependence on temperature (WLF-like versus Arrhenius-like). Consequently, the value of τ_{br} must be determined by accounting for these two possible relaxation processes:

$$\tau_{br} = \left(\frac{1}{\tau_{\mathrm{br,WLF}}} + \frac{1}{\tau_{exchange}} \right)^{-1} \quad (18)$$

with

$$\tau_{br,\mathrm{WLF}} = \tau_{br,\mathrm{WLF}}\ (30\ ^\circ\mathrm{C}) \cdot a_T \quad (19)$$

and $\tau_{exchange}$ defined by eq 17.

In eq 19, the shift factor a_T is determined from eq2 Results obtained with eq 18 are shown in Figure 9e. For the whole range of temperature, in comparison with the best-fit values found for τ_{br} for the higher temperature, while the whole curves G′ and G″ of sample **20k-F10-C4** predicted based on eqs 8−19 are compared to the experimental data in Figure 11. A good agreement is obtained for all temperatures. In Supporting Information, the contribution of each component

https://doi.org/10.1021/acs.macromol.5c03092
Macromolecules 2026, 59, 2818−2834

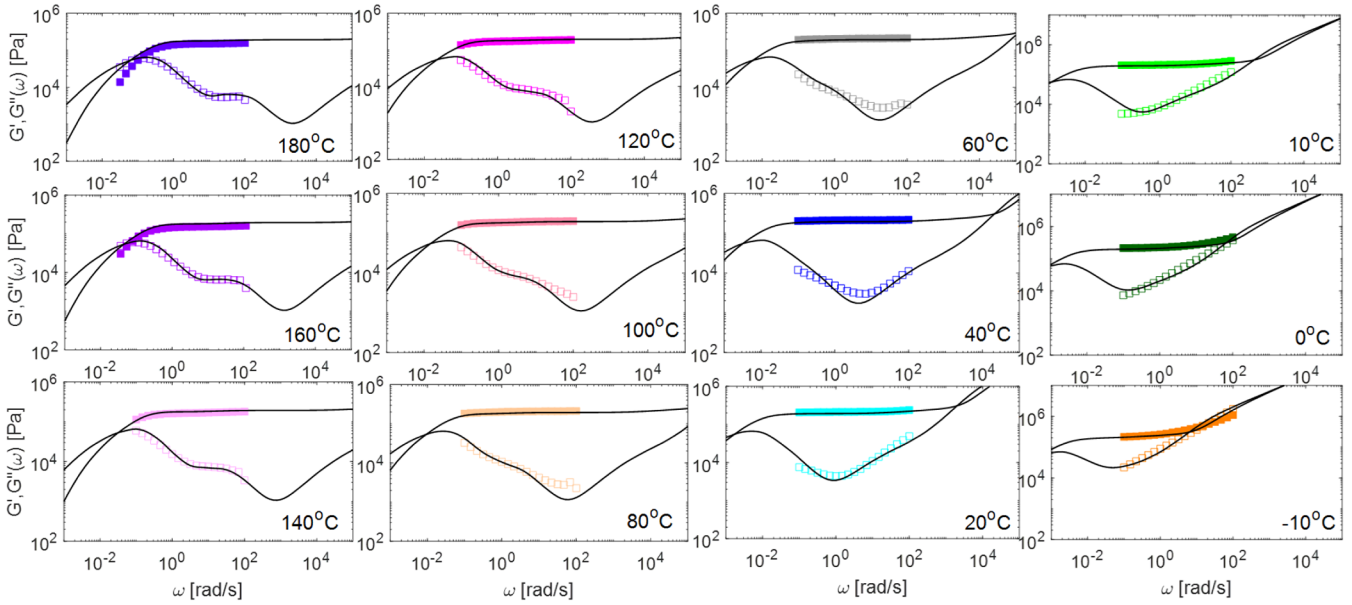

Figure 11. Storage and loss moduli of sample **20k-F10-C4** at different temperatures. Comparison between experimental (symbols) and theoretical (continuous curves) data. The fit parameters used in the model are listed in Table 2.

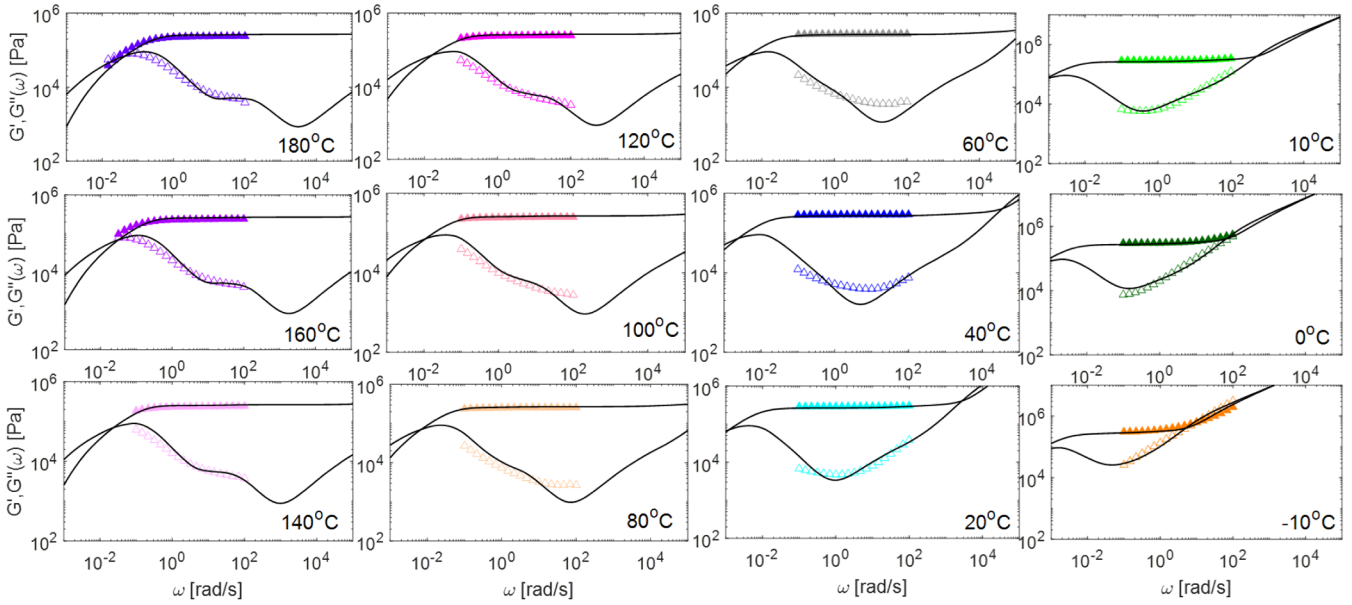

Figure 12. Storage and loss moduli of sample **20K-F10-C10** at different temperatures. Comparison between experimental (symbols) and theoretical (continuous curves) data.

to the storage and loss moduli network is shown at a representative temperature of 120 °C (see Figure S10).

In Section 3.3, we therefore use the proposed model to describe and discuss the viscoelastic response of the different vitrimer samples.

3.3. Influence of Temperature, Molar Mass and Cross-Linking Density on the Vitrimer Dynamics

In this Section, we investigate the influence of the sample composition and temperature on the properties of the vitrimers with the help of our tube model. To investigate the influence of the cross-linking density, we first model and compare the viscoelastic properties of sample **20k-F10-C4** and sample **20k-F10-C10**. Results are shown in Figures 11 and 12, respectively. The best-fit parameters used for their modeling are presented in Table 2.

Table 2. Parameters Used in the Model

Sample name	20k-F10-C2	20k-F10-C4	20k-F10-C10	34k-F10-C2	34k-F10-C4
$M_{xx,\,\text{theoretical}}$ (kg/mol)	5.0	3.0	1.3	5.0	3.0
M_{xx} (kg/mol)	6.5	4.32	3.56	9.1	4.8
$M_{xx,2}$ (kg/mol)	13.5	4.86	3.78	13.5	5.0
$\tau_{exchange,30\ °C}$ (s)	50		81		
$\tau_{br,\text{WLF},30\ °C}$			92		
E_a (kJ/mol)			25		

https://doi.org/10.1021/acs.macromol.5c03092
Macromolecules 2026, 59, 2818−2834

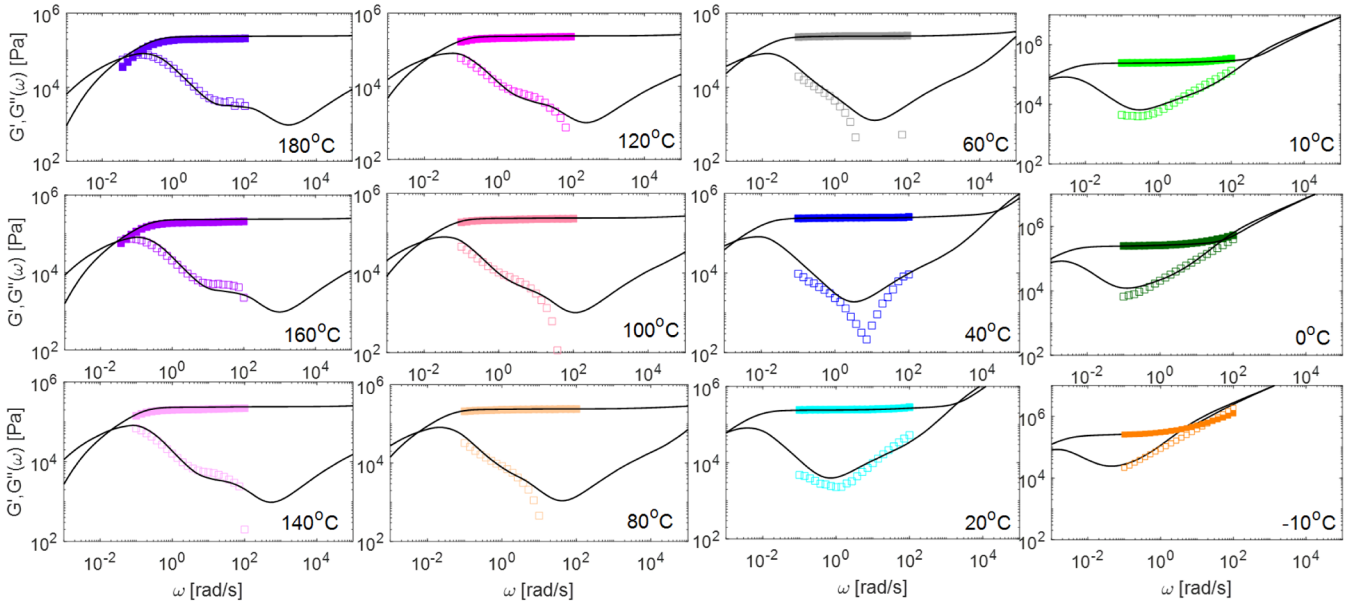

Figure 13. Storage and loss moduli of sample **34K-F10-C4** at different temperatures. Comparison between experimental (symbols) and theoretical (continuous curves) data.

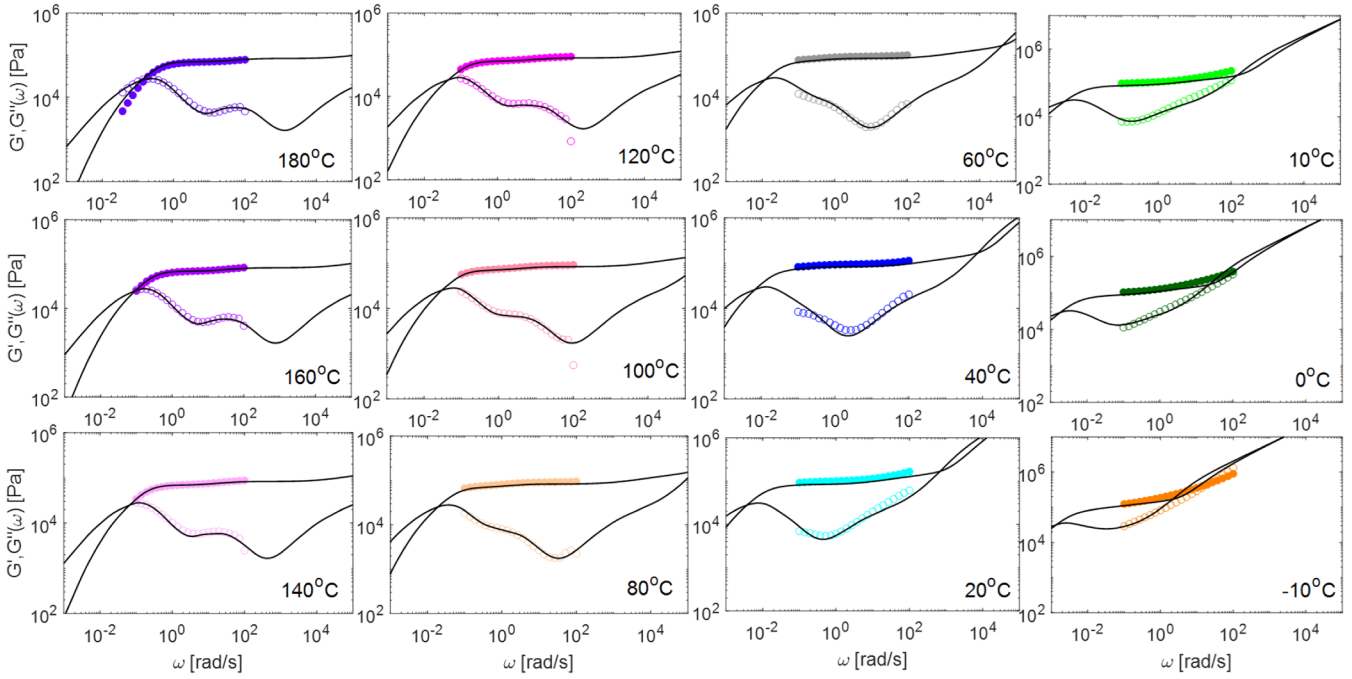

Figure 14. Storage and loss moduli of sample **34k-F10-C2** at different temperatures. Comparison between experimental (symbols) and theoretical (continuous curves) data.

A good description of the experimental data is obtained while keeping the same exchange time of the dynamic covalent bonds at 30 °C and the same temperature dependence for both systems. The equivalence of $\tau_{exchange}$ independently of the cross-linking density is also confirmed in Figure 3a,b, where it was observed that the loss moduli of the different samples superimpose in the frequency region corresponding to the beginning of the network relaxation (between 1 and 10 rad/s). While the exchange times are similar for both systems, their crossover relaxation time increases with the cross-linking density, in agreement with the sticky Rouse model (eq 15). The independence of $\tau_{exchange}$ in function of the cross-linker density differs from refs [33,34]. This may be due to the active participation of the free functional groups to the exchange process, the density of the latter being the same in all vitrimers. Moreover, as already mentioned in Section 3.1.3., the activation energy used to describe the temperature dependence on terminal relaxation peak is found to be the same for all the vitrimers. As discussed in ref 65 this can be attributed to the fact that at the time the vitrimers are relaxing, the delay due to the segmental motion of the chain backbone is negligible compared to the delay due to the exchange dynamics of the cross-linking junctions.

https://doi.org/10.1021/acs.macromol.5c03092
Macromolecules 2026, 59, 2818−2834

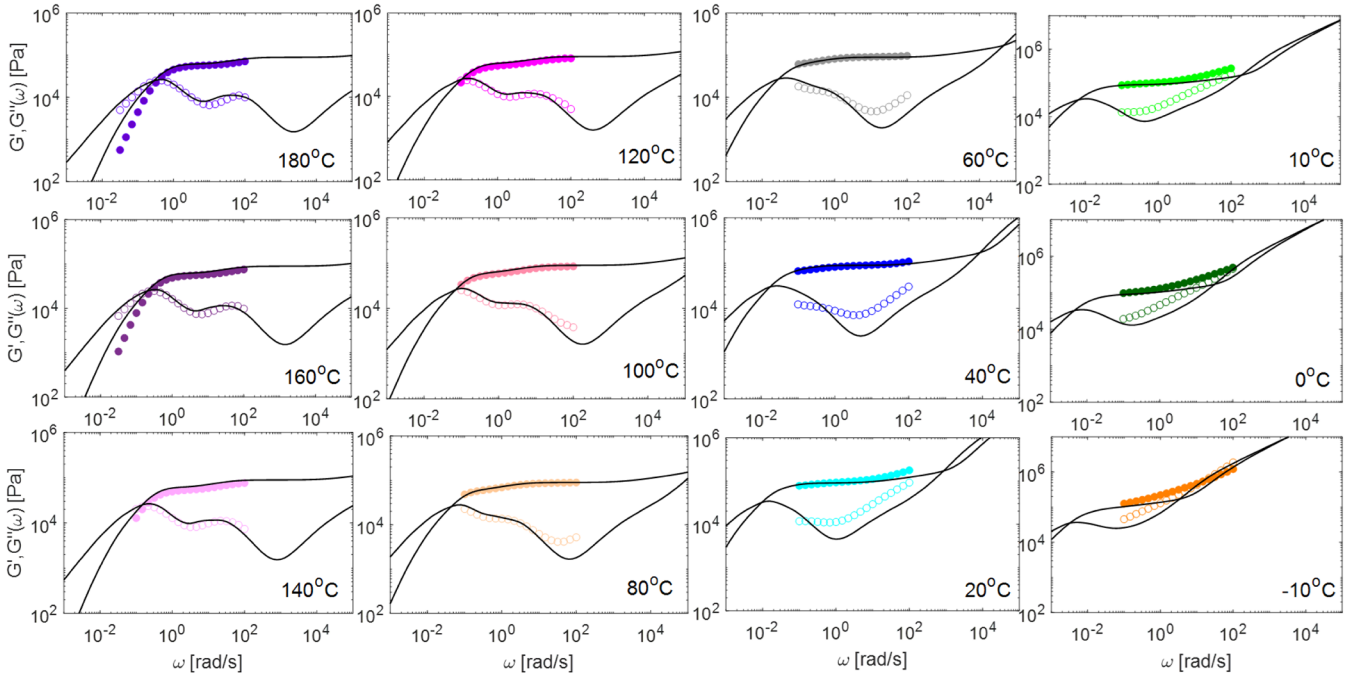

Figure 15. Storage and loss moduli of sample **20K-F10-C2** at different temperatures. Comparison between experimental (symbols) and theoretical (continuous curves) data.

In Table 2, it is seen that the same values of $\tau_{crosslink,30\ °C}$ has been used for the two samples, which indicates that while the probability of finding a chain with only one cross-link is larger for sample **20k-F10-C4** than for sample **20k-F10-C10**, the average molar mass of the complex branches attached to the poorly cross-linked branching point is similar for the two samples.

The other unknown parameters are the mesh-sizes M_{xx} and $M_{xx,2}$. In the specific case of sample **20k-F10-C4**, the values of M_{xx} and $M_{xx,2}$ have been fixed to 4860 g/mol and 4320 g/mol, respectively, based on the best-fitting method. The value of M_{xx} is larger than the theoretical value determined from the synthesis recipe, which is equal to 3000 g/mol. This difference is attributed to the presence of internal loops or other defects in the network. From the value of $M_{xx,2}$ the fraction of molecular strands which relax via the motions of the cross-links loosely connected to the network is estimated to $\left(1 - \sqrt{\frac{M_{xx}}{M_{xx,2}}}\right) = 6$ wt %. This number roughly corresponds to the probability of a branching point to be attached to a chain containing only one cross-link, which has been estimated to 5.6% (see Figure 7c). A similar observation is also made for the other samples. Moreover, with increasing the number of junctions per chain, the value of $M_{xx,2}$ becomes very close to the value of M_{xx}, due to the lower density of poorly trapped cross-links. This suggests that the poorly trapped cross-links are mainly due to the presence of chains with only one effective cross-link (see Figure 10). Such chains are becoming very rare for the samples C4 and C10.

To investigate the influence of the molar mass of the precursors, we then model the viscoelastic properties of the vitrimers built from the longer precursor of mass 34 kg/mol. The data are shown in Figures 13 and 14 for samples **34k-F10-C4** and **34k-F10-C10**, respectively. Here again, a good description of the data is obtained with the same values of E_a and $\tau_{exchange,}30$ °C as for the 20k samples. Thus, again, the exchange dynamics does not seem to depend on the molar mass of the sample. Nevertheless, at same cross-linking density, the terminal relaxation of these longer chains is delayed, as shown in Figure 3c,d for the C4 samples. This is in line with the fact that the vitrimers with the long precursor carry more functional groups and require more time to achieve full relaxation, as described by their sticky Rouse time in eq 15. It is also observed, in Table 2, that the cross-linking efficiency, $1/M_{xx}$, decreases with increasing the molar mass of the precursor.

Finally, if the cross-linker density is largely reduced, as shown in Figures 14 and 15 for the C2 samples, the proportion of dangling ends becomes important, which leads to a larger amount of loosely cross-linked branching points and rather large values of $M_{xx,2}$ (see Table 2). In sample **20k-F10-C2**, many chains contain only two cross-linking junctions, and the network is thus very loose. As shown in Figure 15, larger discrepancies appear between the theoretical and the experimental data for this shorter sample. The validity limit of the approach proposed is reached, as the latter does not account for the possible relaxation of dangling ends composed of several chains.

Thus, from the comparison between experimental and theoretical data, we conclude that the model proposed in the present work is suitable to rationalize the viscoelastic properties of the vitrimers. Its use allowed us to show that for these systems studied, the exchange lifetime of dynamic covalent bonds is independent of the cross-linker density and of the molar mass of the precursors, at least in the studied range. It must be also noted that all the vitrimer samples contain free functional groups or inefficient cross-links along the chain backbone.

Furthermore, the good description of the data validates the dependence on temperature proposed for the different relaxation processes. This provides interesting insight into the origin of the thermal complexity involved in constructing vitrimer master curves.

https://doi.org/10.1021/acs.macromol.5c03092
Macromolecules 2026, 59, 2818−2834

4. CONCLUSION AND OUTLOOK

In this study, small-amplitude oscillatory shear experiments and modeling were combined to investigate the linear viscoelastic properties of low T_g dioxaborolane vitrimers made of P*n*BA precursors of different molar masses with variable cross-linking densities. Thermo-rheological complexity appeared when constructing the master curves via pure WLF or WLF and Arrhenius shifts. To decode this thermal complexity, a TMA model was successfully constructed to catch the essence of the relaxation of these vitrimers. For vitrimers with low cross-linking densities, an intermediate relaxation process is visible, that was attributed to cross-linking points loosely connected to the network that are able to move and relax similarly than a complex branched architecture if the latter process is faster than the bond exchange time. The slower terminal relaxation, detected for all compositions, was well captured by the exchange dynamics of dioxaborolane groups combined with a sticky Rouse model. The bond exchange time was found to be independent of the cross-linker density and of the molar mass of the precursors. Based on the TMA model, we could provide an explanation for the failure of constructing tTS master curves of vitrimers, pointing out the different temperature dependences of the segmental dynamics, of the exchange dynamics of the cross-links, but also of the complex dynamics of the cross-linking points loosely connected to the network. The TMA model shows potential to catch the overall relaxation of other kinds of vitrimers, some of them also displaying an intermediate relaxation peak,[29,66] as it only needs realistic parameters which can be acquired from the data. However, the current study focused on a narrow range of precursor molar masses and constant number of functional groups per chain. It is essential to extend our TMA model to vitrimers with a wider variety of precursor properties and, in particular, to entangled vitrimers. Understanding the nonlinear viscoelastic properties of these specific vitrimers is also important, as it may provide further insights into the coupling between segmental motion and exchange dynamics, as well as industrial processing.

■ ASSOCIATED CONTENT

Supporting Information

The Supporting Information is available free of charge at https://pubs.acs.org/doi/10.1021/acs.macromol.5c03092.

Additional details on the materials, the synthesis, the preparation of the vitrimers, the protocols of measurement with the different techniques, the DSC data, and the theoretical values of the plateau modulus, determined with different approaches (PDF)

■ AUTHOR INFORMATION

Corresponding Author

Evelyne Van Ruymbeke − *Bio- and Soft Matter (BSMA), Institute of Condensed Matter and Nanosciences, Université catholique de Louvain, Louvain-la-Neuve B-1348, Belgium;* orcid.org/0000-0001-7633-0194; Email: Evelyne.vanruymbeke@uclouvain.be

Authors

Hao Wang − *Bio- and Soft Matter (BSMA), Institute of Condensed Matter and Nanosciences, Université catholique de Louvain, Louvain-la-Neuve B-1348, Belgium; South China Advanced Institute for Soft Matter Science and Technology (AISMST), School of Emergent Soft Matter (SESM), South China University of Technology, Guangzhou 510640, P. R. China*

Nuofei Jiang − *Bio- and Soft Matter (BSMA), Institute of Condensed Matter and Nanosciences, Université catholique de Louvain, Louvain-la-Neuve B-1348, Belgium;* orcid.org/0000-0002-6105-354X

Rongchun Zhang − *South China Advanced Institute for Soft Matter Science and Technology (AISMST), School of Emergent Soft Matter (SESM), South China University of Technology, Guangzhou 510640, P. R. China;* orcid.org/0000-0002-2480-2652

Renaud Nicolaÿ − *Chimie Moléculaire, Macromoléculaire, Matériaux, ESPCI Paris, Université PSL, CNRS, Paris 75005, France;* orcid.org/0000-0003-1165-2592

Charles-André Fustin − *Bio- and Soft Matter (BSMA), Institute of Condensed Matter and Nanosciences, Université catholique de Louvain, Louvain-la-Neuve B-1348, Belgium;* orcid.org/0000-0002-3021-5438

Complete contact information is available at: https://pubs.acs.org/10.1021/acs.macromol.5c03092

Notes

The authors declare no competing financial interest.

■ ACKNOWLEDGMENTS

We thank Prof. Quan Chen for fruitful discussions on this work. Hao Wang thank the financial support from the China Scholarship Council (CSC). Evelyne van Ruymbeke is a Senior Research Associate of the FRS-FNRS.

■ REFERENCES

(1) De Lucca Freitas, L. L.; Stadler, R. Thermoplastic Elastomers by Hydrogen Bonding. 3. Interrelations between Molecular Parameters and Rheological Properties. *Macromolecules* **1987**, *20* (10), 2478−2485.

(2) Ahmadi, M.; Jangizehi, A.; van Ruymbeke, E.; Seiffert, S. Deconvolution of the Effects of Binary Associations and Collective Assemblies on the Rheological Properties of Entangled Side-Chain Supramolecular Polymer Networks. *Macromolecules* **2019**, *52* (14), 5255−5267.

(3) Chen, Q.; Tudryn, G. J.; Colby, R. H. Ionomer Dynamics and the Sticky Rouse Modela). *J. Rheol.* **2013**, *57* (5), 1441−1462.

(4) Zhang, L.; Brostowitz, N. R.; Cavicchi, K. A.; Weiss, R. A. Perspective: Ionomer Research and Applications. *Macromol. React. Eng.* **2014**, *8* (2), 81−99.

(5) Burnworth, M.; Tang, L.; Kumpfer, J. R.; Duncan, A. J.; Beyer, F. L.; Fiore, G. L.; Rowan, S. J.; Weder, C. Optically Healable Supramolecular Polymers. *Nature* **2011**, *472* (7343), 334−337.

(6) Zhuge, F.; Brassinne, J.; Fustin, C.-A.; van Ruymbeke, E.; Gohy, J.-F. Synthesis and Rheology of Bulk Metallo-Supramolecular Polymers from Telechelic Entangled Precursors. *Macromolecules* **2017**, *50* (13), 5165−5175.

(7) Chen, X.; Dam, M. A.; Ono, K.; Mal, A.; Shen, H.; Nutt, S. R.; Sheran, K.; Wudl, F. A Thermally Re-Mendable Cross-Linked Polymeric Material. *Science* **2002**, *295* (5560), 1698−1702.

(8) Scheutz, G. M.; Lessard, J. J.; Sims, M. B.; Sumerlin, B. S. Adaptable Crosslinks in Polymeric Materials: Resolving the Intersection of Thermoplastics and Thermosets. *J. Am. Chem. Soc.* **2019**, *141* (41), 16181−16196.

(9) Adzima, B. J.; Aguirre, H. A.; Kloxin, C. J.; Scott, T. F.; Bowman, C. N. Rheological and Chemical Analysis of Reverse Gelation in a Covalently Cross-Linked Diels−Alder Polymer Network. *Macromolecules* **2008**, *41* (23), 9112−9117.

(10) Zhang, Y.; Broekhuis, A. A.; Picchioni, F. Thermally Self-Healing Polymeric Materials: The Next Step to Recycling Thermoset Polymers? *Macromolecules* **2009**, *42* (6), 1906−1912.
(11) Montarnal, D.; Capelot, M.; Tournilhac, F.; Leibler, L. Silica-Like Malleable Materials from Permanent Organic Networks. *Science* **2011**, *334* (6058), 965−968.
(12) Capelot, M.; Unterlass, M. M.; Tournilhac, F.; Leibler, L. Catalytic Control of the Vitrimer Glass Transition. *ACS Macro Lett.* **2012**, *1* (7), 789−792.
(13) Yu, S.; Zhang, R.; Wu, Q.; Chen, T.; Sun, P. Bio-Inspired High-Performance and Recyclable Cross-Linked Polymers. *Adv. Mater.* **2013**, *25* (35), 4912−4917.
(14) Van Zee, N. J.; Nicolaÿ, R. Vitrimers: Permanently Crosslinked Polymers with Dynamic Network Topology. *Prog. Polym. Sci.* **2020**, *104*, 101233.
(15) Van Zee, N. J.; Nicolaÿ, R. Vitrimer Chemistry and Applications. *Macromolecular Engineering*; Wiley, 2022, pp. 1−38. DOI: .
(16) Röttger, M.; Domenech, T.; van der Weegen, R.; Breuillac, A.; Nicolaÿ, R.; Leibler, L. High-Performance Vitrimers from Commodity Thermoplastics through Dioxaborolane Metathesis. *Science* **2017**, *356* (6333), 62−65.
(17) Breuillac, A.; Caffy, F.; Vialon, T.; Nicolaÿ, R. Functionalization of Polyisoprene and Polystyrene via Reactive Processing Using Azidoformate Grafting Agents, and Its Application to the Synthesis of Dioxaborolane-Based Polyisoprene Vitrimers. *Polym. Chem.* **2020**, *11* (40), 6479−6491.
(18) Tretbar, C.; Castro, J.; Yokoyama, K.; Guan, Z. Fluoride-Catalyzed Siloxane Exchange as a Robust Dynamic Chemistry for High-Performance Vitrimers. *Adv. Mater.* **2023**, *35* (28), 2303280.
(19) Clarke, R. W.; Sandmeier, T.; Franklin, K. A.; Reich, D.; Zhang, X.; Vengallur, N.; Patra, T. K.; Tannenbaum, R. J.; Adhikari, S.; Kumar, S. K.; Rovis, T.; Chen, E. Y.-X. Dynamic Crosslinking Compatibilizes Immiscible Mixed Plastics. *Nature* **2023**, *616* (7958), 731−739.
(20) Vialon, T.; Sun, H.; Formon, G. J. M.; Galanopoulo, P.; Guibert, C.; Averseng, F.; Rager, M.-N.; Percot, A.; Guillaneuf, Y.; Van Zee, N. J.; Nicolaÿ, R. Upcycling Polyolefin Blends into High-Performance Materials by Exploiting Azidotriazine Chemistry Using Reactive Extrusion. *J. Am. Chem. Soc.* **2024**, *146* (4), 2673−2684.
(21) Castro, J.; Westworth, X.; Shrestha, R.; Yokoyama, K.; Guan, Z. Efficient and Robust Dynamic Crosslinking for Compatibilizing Immiscible Mixed Plastics through In Situ Generated Singlet Nitrenes. *Adv. Mater.* **2024**, *36* (32), 2406203.
(22) Ferry, J. D. *Viscoelastic Properties of Polymers*, 3d ed.; Wiley: New York, 1980.
(23) Meng, F.; Saed, M. O.; Terentjev, E. M. Rheology of Vitrimers. *Nat. Commun.* **2022**, *13* (1), 5753.
(24) Wu, S.; Yang, H.; Huang, S.; Chen, Q. Relationship between Reaction Kinetics and Chain Dynamics of Vitrimers Based on Dioxaborolane Metathesis. *Macromolecules* **2020**, *53* (4), 1180−1190.
(25) Perego, A.; Lazarenko, D.; Cloitre, M.; Khabaz, F. Microscopic Dynamics and Viscoelasticity of Vitrimers. *Macromolecules* **2022**, *55* (17), 7605−7613.
(26) Ge, S.; Evans, C. M. Influence of Segmental Dynamics on Bond Exchange in Imine Vitrimers with Different Polymer Backbones and Cross-Linkers. *Macromolecules* **2025**, *58* (8), 4043−4058.
(27) Zhao, H.; Li, Z.; Zhan, S.; Yue, T.; Qu, J.; Li, H.; Zhang, L.; Ganesan, V.; Liu, J. Role of Dynamic Covalent Bond Density on the Structure and Properties of Vitrimers. *Macromolecules* **2024**, *57* (23), 11296−11310.
(28) Ricarte, R. G.; Shanbhag, S. Unentangled Vitrimer Melts: Interplay between Chain Relaxation and Cross-Link Exchange Controls Linear Rheology. *Macromolecules* **2021**, *54* (7), 3304−3320.
(29) Snijkers, F.; Pasquino, R.; Maffezzoli, A. Curing and Viscoelasticity of Vitrimers. *Soft Matter* **2017**, *13* (1), 258−268.
(30) Stukenbroeker, T.; Wang, W.; Winne, J. M.; Prez, F. E. D.; Nicolaÿ, R.; Leibler, L. Polydimethylsiloxane Quenchable Vitrimers. *Polym. Chem.* **2017**, *8* (43), 6590−6593.
(31) Chen, Q.; Gong, S.; Moll, J.; Zhao, D.; Kumar, S. K.; Colby, R. H. Mechanical Reinforcement of Polymer Nanocomposites from Percolation of a Nanoparticle Network. *ACS Macro Lett.* **2015**, *4* (4), 398−402.
(32) Goldansaz, H.; Fustin, C.-A.; Wübbenhorst, M.; van Ruymbeke, E. How Supramolecular Assemblies Control Dynamics of Associative Polymers: Toward a General Picture. *Macromolecules* **2016**, *49* (5), 1890−1902.
(33) Soman, B.; Evans, M. C. Effect of Precise Linker Length, Bond Density, and Broad Temperature Window on the Rheological Properties of Ethylene Vitrimers. *Soft Matter* **2021**, *17* (13), 3569−3577.
(34) Cromwell, O. R.; Chung, J.; Guan, Z. Malleable and Self-Healing Covalent Polymer Networks through Tunable Dynamic Boronic Ester Bonds. *J. Am. Chem. Soc.* **2015**, *137* (20), 6492−6495.
(35) Denissen, W.; Rivero, G.; Nicolaÿ, R.; Leibler, L.; Winne, J. M.; Du Prez, F. E. Vinylogous Urethane Vitrimers. *Adv. Funct. Mater.* **2015**, *25* (16), 2451−2457.
(36) Lessard, J. J.; Stewart, K. A.; Sumerlin, B. S. Controlling Dynamics of Associative Networks through Primary Chain Length. *Macromolecules* **2022**, *55* (22), 10052−10061.
(37) Rubinstein, M.; Helfand, E.; Pearson, D. S. Theory of Polydispersity Effects of Polymer Rheology: Binary Distribution of Molecular Weights. *Macromolecules* **1987**, *20* (4), 822−829.
(38) Jiang, N.; Zhang, H.; Tang, P.; Yang, Y. Linear Viscoelasticity of Associative Polymers: Sticky Rouse Model and the Role of Bridges. *Macromolecules* **2020**, *53* (9), 3438−3451.
(39) Leibler, L.; Rubinstein, M.; Colby, R. H. Dynamics of Reversible Networks. *Macromolecules* **1991**, *24* (16), 4701−4707.
(40) Rubinstein, M.; Semenov, A. N. Dynamics of Entangled Solutions of Associating Polymers. *Macromolecules* **2001**, *34* (4), 1058−1068.
(41) Luo, J.; Zhao, X.; Ju, H.; Chen, X.; Zhao, S.; Demchuk, Z.; Li, B.; Bocharova, V.; Carrillo, J.-M. Y.; Keum, J. K.; Xu, S.; Sokolov, A. P.; Chen, J.; Cao, P.-F. Highly Recyclable and Tough Elastic Vitrimers from a Defined Polydimethylsiloxane Network. *Angew. Chem. Int. Ed.* **2023**, *62* (47), No. e202310989.
(42) Lessard, J. J.; Scheutz, G. M.; Sung, S. H.; Lantz, K. A.; Epps, T. H. I.; Sumerlin, B. S. Block Copolymer Vitrimers. *J. Am. Chem. Soc.* **2020**, *142* (1), 283−289.
(43) *Polymer Handbook*,Brandrup, J.; Immergut, E. H.; Grulke, E. A., 4th ed.Eds.;Wiley: New York, 1999.
(44) van Ruymbeke, E.; Bailly, C.; Keunings, R.; Vlassopoulos, D. A General Methodology to Predict the Linear Rheology of Branched Polymers. *Macromolecules* **2006**, *39* (18), 6248−6259.
(45) Hammer, L.; Nicolaÿ, R. Interpenetrating Vitrimers Based on Dioxaborolane Metathesis and Imine-Aldehyde Exchange. *Polym. Chem.* **2025**, *16* (44), 4843−4851.
(46) Finch, A.; Lockhart, J. C. 721. Cyclic Boronates and Their Amine Complexes. *J. Chem. Soc.* **1962**, 3723.
(47) Maaz, M.; Riba-Bremerch, A.; Guibert, C.; Van Zee, N. J.; Nicolaÿ, R. Synthesis of Polyethylene Vitrimers in a Single Step: Consequences of Graft Structure, Reactive Extrusion Conditions, and Processing Aids. *Macromolecules* **2021**, *54* (5), 2213−2225.
(48) Li, Y.; Pyromali, C.; Zhuge, F.; Fustin, C.-A.; Gohy, J.-F.; Vlassopoulos, D.; van Ruymbeke, E. Dynamics of Entangled Metallosupramolecular Polymer Networks Combining Stickers with Different Lifetimes. *J. Rheol.* **2022**, *66* (6), 1203−1220.
(49) Ruymbeke, E. V.; Muliawan, E. B.; Vlassopoulos, D.; Gao, H.; Matyjaszewski, K. Melt Rheology of Star Polymers with Large Number of Small Arms, Prepared by Crosslinking Poly(*n*-Butyl Acrylate) Macromonomers via ATRP. *Eur. Polym. J.* **2011**, *47* (4), 746−751.
(50) Zhuge, F.; Hawke, L. G. D.; Fustin, C.-A.; Gohy, J.-F.; van Ruymbeke, E. Decoding the Linear Viscoelastic Properties of Model Telechelic Metallo-Supramolecular Polymers. *J. Rheol.* **2017**, *61* (6), 1245−1262.
(51) Ishibashi, J. S. A.; Pierce, I. C.; Chang, A. B.; Zografos, A.; El-Zaatari, B. M.; Fang, Y.; Weigand, S. J.; Bates, F. S.; Kalow, J. A.

Mechanical and Structural Consequences of Associative Dynamic Cross-Linking in Acrylic Diblock Copolymers. *Macromolecules* **2021**, *54* (9), 3972−3986.
(52) Rubinstein, M.; Colby, R. H. *Polymer Physics*; Oxford University Press: Oxford ; New York, 2003.
(53) Williams, M. L.; Landel, R. F.; Ferry, J. D. The Temperature Dependence of Relaxation Mechanisms in Amorphous Polymers and Other Glass-Forming Liquids. *J. Am. Chem. Soc.* **1955**, *77* (14), 3701−3707.
(54) Kwei, T. K. Standard Pressure—Volume—Temperature Data for Polymers, by Paul Zoller and David J. Walsh, Technomic Publ. Co., Lancaster, Pa, 1995. *J. Polym. Sci., Part A:Polym. Chem.* **1996**, *34* (7), 1365−1365.
(55) Martins, M. L.; Zhao, X.; Demchuk, Z.; Luo, J.; Carden, G. P.; Toleutay, G.; Sokolov, A. P. Viscoelasticity of Polymers with Dynamic Covalent Bonds: Concepts and Misconceptions. *Macromolecules* **2023**, *56* (21), 8688−8696.
(56) Zhang, Z.; Huang, C.; Weiss, R. A.; Chen, Q. Association Energy in Strongly Associative Polymers. *J. Rheol.* **2017**, *61* (6), 1199−1207.
(57) Ghosh, A.; Schweizer, K. S. Physical Bond Breaking in Associating Copolymer Liquids. *ACS Macro Lett.* **2021**, *10* (1), 122−128.
(58) Röttger, M.; Domenech, T.; van der Weegen, R.; Breuillac, A.; Nicolaÿ, R.; Leibler, L. High- performance vitrimers from commodity thermoplastics through dioxaborolane metathesis. *Science* **2017**, *356*, 62−65.
(59) Ricarte, R. G.; Shanbhag, S.; Ezzeddine, D.; Barzycki, D.; Fay, K. Time-Temperature Superposition of Polybutadiene Vitrimers. *Macromolecules* **2023**, *56* (17), 6806−6817.
(60) Hayashi, M.; Ricarte, R. G. Towards the next development of vitrimers: Recent key topics for the practical application and understanding of the fundamental physics. *Prog. Polym. Sci.* **2025**, *170*, 102026.
(61) Schwarzl, F. R. Numerical Calculation of Storage and Loss Modulus from Stress Relaxation Data for Linear Viscoelastic Materials. *Rheol. Acta* **1971**, *10* (2), 165−173.
(62) Hawke, L. G. D.; Ahmadi, M.; Goldansaz, H.; van Ruymbeke, E. Viscoelastic Properties of Linear Associating Poly(n-Butyl Acrylate) Chains. *J. Rheol.* **2016**, *60* (2), 297−310.
(63) Stukalin, E. B.; Cai, L.-H.; Kumar, N. A.; Leibler, L.; Rubinstein, M. Self-Healing of Unentangled Polymer Networks with Reversible Bonds. *Macromolecules* **2013**, *46* (18), 7525−7541.
(64) Chen, Q.; Huang, C.; Weiss, R. A.; Colby, R. H. Viscoelasticity of Reversible Gelation for Ionomers. *Macromolecules* **2015**, *48* (4), 1221−1230.
(65) de Wergifosse, P.; Lyons, R.; Fustin, C. -A.; van Ruymbeke, E. Viscoelastic Properties of Metallo- Supramolecular Networks: Relationship Between Sticker/Entanglement Dynamics and Terminal Relaxation. *Macromolecules* **2025**, *58* (1), 222−239.
(66) Stukenbroeker, T.; Wang, W.; Winne, J. M.; Du Prez, F. E.; Nicolaÿ, R.; Leibler, L. Polydimethylsiloxane quenchable vitrimers. *Polym. Chem.* **2017**, *8* (43), 6590−6593.

https://doi.org/10.1021/acs.macromol.5c03092
Macromolecules 2026, 59, 2818−2834